

Therapy-induced tumour secretomes promote resistance and tumour progression

Anna C. Obenauf¹, Yilong Zou^{1,2*}, Andrew L. Ji^{1*}, Sakari Vanharanta^{1,3}, Weiping Shu¹, Hubing Shi⁴, Xiangju Kong⁴, Marcus C. Bosenberg^{5,6}, Thomas Wiesner⁷, Neal Rosen⁸, Roger S. Lo⁴ & Joan Massagué¹

Drug resistance invariably limits the clinical efficacy of targeted therapy with kinase inhibitors against cancer^{1,2}. Here we show that targeted therapy with BRAF, ALK or EGFR kinase inhibitors induces a complex network of secreted signals in drug-stressed human and mouse melanoma and human lung adenocarcinoma cells. This therapy-induced secretome stimulates the outgrowth, dissemination and metastasis of drug-resistant cancer cell clones and supports the survival of drug-sensitive cancer cells, contributing to incomplete tumour regression. The tumour-promoting secretome of melanoma cells treated with the kinase inhibitor vemurafenib is driven by down-regulation of the transcription factor FRA1. *In situ* transcriptome analysis of drug-resistant melanoma cells responding to the regressing tumour microenvironment revealed hyperactivation of several signalling pathways, most prominently the AKT pathway. Dual inhibition of RAF and the PI(3)K/AKT/mTOR intracellular signalling pathways blunted the outgrowth of the drug-resistant cell population in *BRAF* mutant human melanoma, suggesting this combination therapy as a strategy against tumour relapse. Thus, therapeutic inhibition of oncogenic drivers induces vast secretome changes in drug-sensitive cancer cells, paradoxically establishing a tumour microenvironment that supports the expansion of drug-resistant clones, but is susceptible to combination therapy.

Kinase inhibitors such as vemurafenib, erlotinib or crizotinib have shown clinical efficacy in melanoma with *BRAF* mutations, or in lung adenocarcinoma with *EGFR* mutations or *ALK* translocations, respectively^{3–6}. Although complete responses are rare, the vast majority of patients show partial tumour regression or disease stabilization. However, drug resistance invariably develops, and most patients progress within 6–12 months^{3–16}, representing a common complication of targeted therapies that hampers long-term treatment success. The rapid emergence of clinical drug resistance may be facilitated by a small number of pre-existing cancer cells that are intrinsically resistant or poised to adapt to drug treatment quickly^{17–19}. How these minority clones of drug-resistant cells react to the marked changes in the microenvironment during tumour regression is not known. A better understanding of this process could lead to treatments that improve the efficacy of current targeted anti-cancer drugs.

To model therapeutic targeting of heterogeneous tumour cell populations *in vivo*, we mixed a small percentage of vemurafenib-resistant A375 human melanoma cells (A375^R), labelled with a TK-GFP-luciferase (TGL) vector, together with mostly non-labelled, vemurafenib-sensitive A375 cells, and injected the admixture (A375/A375^R, 99.95/0.05%) subcutaneously in mice (Extended Data Fig. 1a). After the tumours were established, we treated the mice with vemurafenib or vehicle, and monitored the growth of resistant cells by bioluminescent imaging (BLI) *in vivo* (Fig. 1a). Although vemurafenib treatment decreased the volume of sensitive tumours (A375 alone) (Extended Data Fig. 1b), the

number of admixed resistant cells in regressing tumours (A375/A375^R) significantly increased compared to vehicle-treated controls (Fig. 1b). Green fluorescent protein (GFP) staining confirmed increased numbers of resistant cells in regressing tumours, and EdU or BrdU staining confirmed their increased proliferation rate compared to the vehicle-treated controls (Fig. 1c and Extended Data Fig. 1c, d). Tumours comprising only resistant cells showed no growth difference when treated with vehicle or vemurafenib (Fig. 1d), indicating that the growth advantage of resistant cells in regressing tumours was not caused by direct effects of vemurafenib on cancer or stromal cells.

Treatment of mixed A375 and A375^R tumours with dabrafenib, another BRAF inhibitor (RAF*i*), or doxycycline-induced knockdown of *BRAF* had similar effects (Extended Data Fig. 1e–g). In line with these findings, A375^R cells co-implanted with other vemurafenib-sensitive melanoma cell lines (Colo800, LOX and UACC62) also showed an up to eightfold growth increase compared to vehicle-treated control groups (Fig. 1e). Growth acceleration of the resistant population in a regressing tumour was also observed in the patient-derived⁸ melanoma cell line M249 and its vemurafenib-resistant derivative M249^{R4}, driven by an *NRAS* mutation, a clinically relevant resistance mechanism (Fig. 1e and Extended Data Fig. 1h). In immunocompetent mice, vemurafenib treatment of tumours formed by melanoma cell lines derived from *Braf*^{V600E} *Cdkn2a*^{-/-} *Pten*^{-/-} mice (YUMM1.1, YUMM1.7) also promoted growth of the admixed vemurafenib-resistant cells (YUMM1.7^R, B16) (Extended Data Fig. 1i, j).

Crizotinib- or erlotinib-treated mice containing tumours formed by *ALK*-driven (H3122) or *EGFR*-driven (HCC827) human lung adenocarcinoma cells, respectively, admixed with minority clones of intrinsically resistant cells from the same cell lineage (lung adenocarcinoma cells H2030 and PC9) or melanoma cells (A375^R) also led to increased outgrowth of the resistant cells (Fig. 1e and Extended Data Fig. 1k–m). Local growth acceleration of resistant cells in the regressing subcutaneous tumours resulted in higher lung metastatic burden (Fig. 1f). Thus, drug-resistant cancer cells benefit from therapeutic targeting of surrounding drug-sensitive cells.

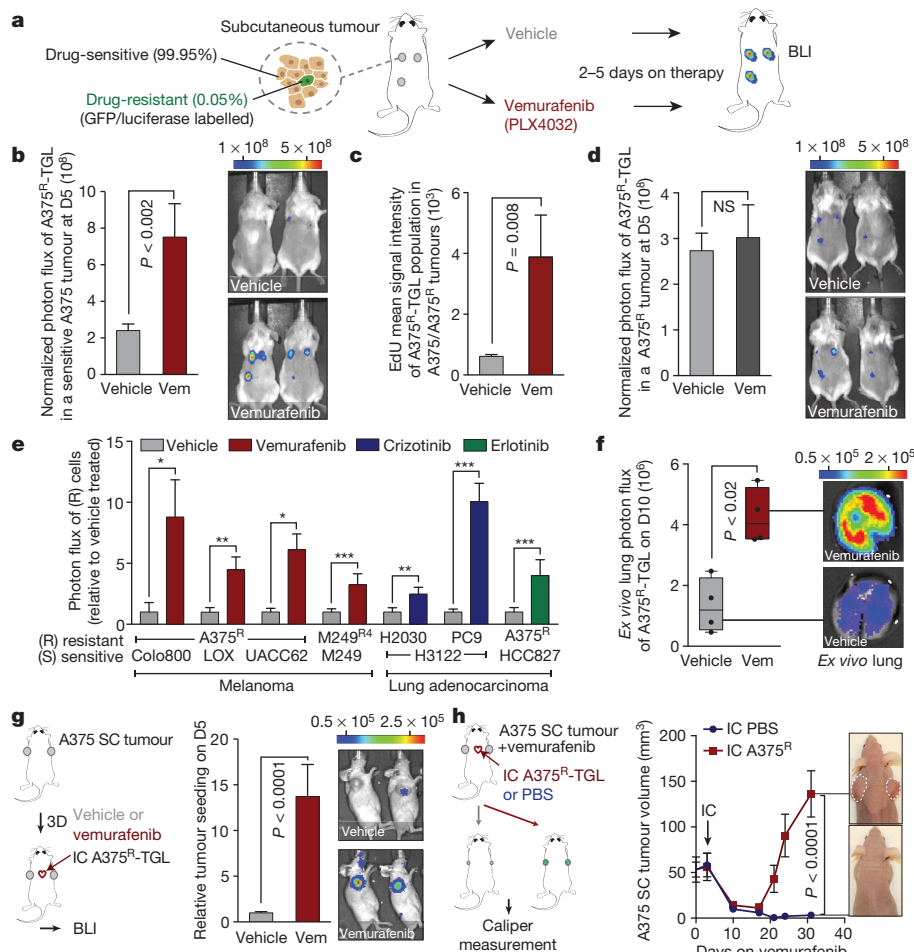
Circulating tumour cells can infiltrate and colonize tumours. This phenomenon, termed self-seeding²⁰, may contribute to the distribution of resistant clones to several metastatic sites. Mice implanted with sensitive A375 tumours were treated with vehicle or vemurafenib, and intracardially injected with TGL-labelled A375^R cells (Fig. 1g). A375^R cells were more efficiently attracted to vemurafenib-treated regressing tumours compared to vehicle-treated controls, with 95% (21 out of 22) and 12.5% (2 out of 16) efficiency, respectively, exhibiting substantial accumulation of resistant cells in regressing tumours by day 5 (Fig. 1g and Extended Data Fig. 1n). To evaluate the contribution of seeding by resistant circulating tumour cells to disease relapse, we intracardially injected resistant A375^R cells or vehicle into tumour-bearing mice and compared

¹Cancer Biology and Genetics Program, Memorial Sloan Kettering Cancer Center, New York, New York 10065, USA. ²Gerstner Sloan Kettering School of Biomedical Sciences, Memorial Sloan Kettering Cancer Center, New York, New York 10065, USA. ³MRC Cancer Unit, University of Cambridge, Cambridge CB2 0XZ, UK. ⁴Division of Dermatology, Department of Medicine and Jonsson Comprehensive Cancer Center, University of California, Los Angeles, California 90095, USA. ⁵Department of Pathology, Yale University School of Medicine, New Haven, Connecticut 06520, USA. ⁶Department of Dermatology, Yale University School of Medicine, New Haven, Connecticut 06520, USA. ⁷Human Oncology and Pathogenesis Program, Memorial Sloan Kettering Cancer Center, New York, New York 10065, USA. ⁸Molecular Pharmacology and Chemistry Program, Memorial Sloan Kettering Cancer Center, New York, New York 10065, USA.

*These authors contributed equally to this work.

Figure 1 | The regressing tumour microenvironment stimulates the outgrowth, infiltration and metastasis of drug-resistant clones.

a, Schematic of the experimental set-up. **b**, Bioluminescent signal of drug-resistant A375^R-TGL cells in vemurafenib-sensitive, A375 tumours, treated with vehicle or vemurafenib for 5 days (vehicle, *n* = 36; vemurafenib, *n* = 15 tumours). **d**, day. **c**, EdU incorporation in A375^R-TGL cells in A375/A375^R-TGL tumours treated with vehicle or vemurafenib for 4 days, as determined by FACS (vehicle, *n* = 8; vemurafenib, *n* = 6 tumours). **d**, Bioluminescent signal of A375^R-TGL tumours alone, treated with vehicle or vemurafenib for 5 days (vehicle, *n* = 38; vemurafenib, *n* = 15 tumours). **e**, Bioluminescent signal of TGL-expressing drug-resistant cancer cells (A375^R, M249^{R4}, PC9 and H2030) in drug-sensitive tumours (Colo800, LOX, UACC62, M249, H3122 and HCC827) treated with vehicle or drugs (vemurafenib, crizotinib and erlotinib) for 5 days (*n* (from left to right on the graph) = 6, 7, 12, 12, 9, 9, 25, 26, 9, 12, 12, 12, 16 and 11 tumours). **f**, Spontaneous lung metastasis by A375^R cells in mice bearing A375/A375^R-TGL tumours treated with vehicle or vemurafenib (10 days), visualized by BLI (*n* = 4). **g**, Seeding of A375^R-TGL cells from the circulation to unlabelled, subcutaneous (SC) A375 tumours of mice treated with vehicle or vemurafenib. Signal in the tumour was quantified by BLI (vehicle, *n* = 30; vemurafenib, *n* = 34 tumours; three independent experiments combined). IC, intracardiac. **h**, Treatment response, determined by tumour size, of subcutaneous A375 tumours allowed to be seeded by A375^R-TGL cells from the circulation or mock injected (vehicle, *n* = 16; vemurafenib, *n* = 8 tumours). Data in **b–e**, **g**, **h** are mean and s.e.m.; in **f** the centre line is median, whiskers are minimum and maximum values. **P* < 0.05, ***P* < 0.01, ****P* < 0.001, two-tailed Mann-Whitney *U* test. NS, not significant.



the tumour volume during vemurafenib treatment (Fig. 1h). Whereas the unseeded tumours in the control group showed extensive tumour regression, seeding by A375^R cells led to rapid tumour relapse (Fig. 1h). These results suggest that tumours regressing on targeted therapy are potent attractors of resistant circulating tumour cells that may contribute to rapid tumour progression.

Tumours consist of a complex microenvironment composed of immune, stromal and cancer cells²¹. Soluble mediators from this microenvironment can foster cancer growth and therapy resistance^{13,14,22–24}. Considering that drug-sensitive cancer cells are the main population affected by targeted therapy, we proposed that signals derived from sensitive cancer cells in response to kinase inhibitors drive the outgrowth of drug-resistant cells. To test this hypothesis, we established an *in vitro* co-culture system and monitored the growth of TGL-expressing resistant cells (A375^R, H2030) in the absence or presence of sensitive cells treated with kinase inhibitors or vehicle (Fig. 2a). Mimicking our *in vivo* findings, co-culture with vemurafenib-, crizotinib- or erlotinib-treated sensitive cells significantly enhanced the growth of resistant cancer cells (Fig. 2a and Extended Data Fig. 2a–c).

We derived conditioned media (CM) from vemurafenib-sensitive melanoma cells cultured in the absence (CM-vehicle) or presence of vemurafenib (CM-vemurafenib). CM-vemurafenib accelerated the proliferation of drug-resistant cells, with different clinically relevant resistance mechanisms, as determined by cell viability assays and Ki67 staining (Fig. 2b and Extended Data Fig. 2d–f). Similarly, conditioned media from crizotinib- or erlotinib-treated sensitive lung adenocarcinoma cells stimulated proliferation of lung adenocarcinoma cells with intrinsic or

acquired resistance (Fig. 2c) and across different cell lineages (Extended Data Fig. 2g). In addition, CM-vemurafenib elicited increased cell migration in transwell migration and monolayer gap-closing assays (Fig. 2d and Extended Data Fig. 2h–k). CM-vemurafenib was also active on vemurafenib-sensitive cancer cells, increasing survival and suppressing the apoptotic caspase activity up to 100-fold in these cells when treated with vemurafenib *in vitro* (Fig. 2e, f). Because all biologically active conditioned media was collected before cell death or senescence, it is likely that the secretome is actively produced as a result of oncogene inhibition (Extended Data Fig. 2l, m). These results demonstrate that *BRAF*, *ALK* and *EGFR* mutant cells respond to therapeutic stress under targeted therapy by secreting factors that support the survival of drug-sensitive cells and accelerate the growth of drug-resistant minority clones. The effects of this reactive secretome may augment previously reported resistance mechanisms including relief of feedback inhibition of intracellular signalling^{11,25}, upregulation of receptor tyrosine kinases²⁶, or the supply of stromal cytokines¹⁴ that protect the drug-sensitive cells.

To identify relevant components and regulators of the reactive secretome, we analysed gene expression changes in sensitive A375 melanoma cells at different time points after vemurafenib exposure *in vitro*. After 6 h on vemurafenib, 473 genes showed altered expression, and pathway analysis revealed that these genes were enriched for transcriptional regulators (Fig. 3a, b, Extended Data Fig. 3a, b and Supplementary Table 1). After 48 h, more than one-third of the transcriptome was differentially expressed (>5,000 genes; 405 genes encoding for proteins in the extracellular region, Gene Ontology (GO) accession 0005576), significantly overlapping with the gene expression changes of A375

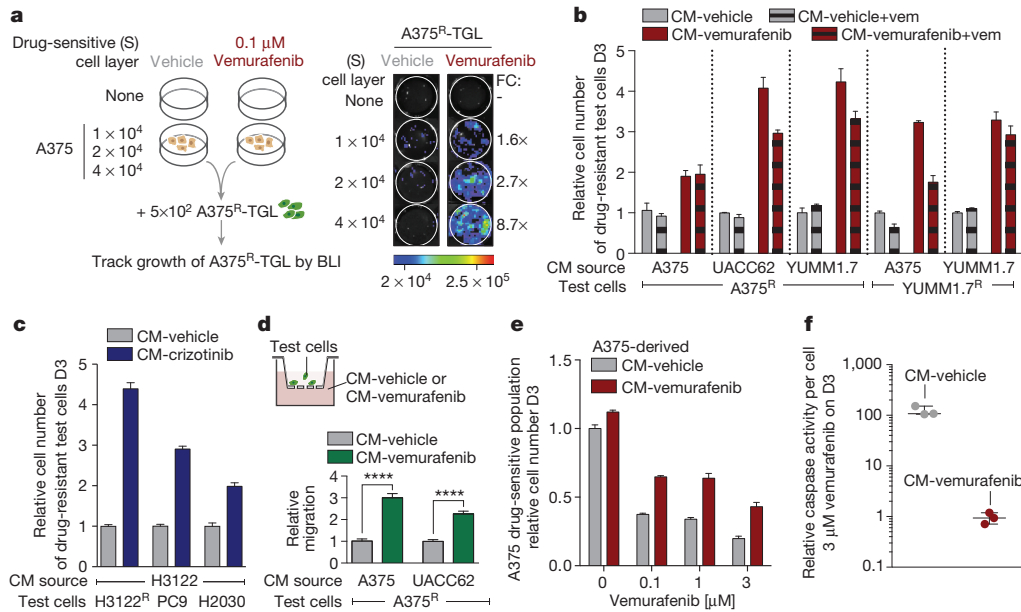


Figure 2 | The secretome of RAF and ALK inhibitor-treated tumour cells increases proliferation and migration of drug-resistant cells and supports the survival of drug-sensitive cells. **a**, Schematic (left) and representative BLI images (right) after 7 days of co-culture. Average fold change (FC) of BLI signal from A375^R-TGL cells in vemurafenib-treated wells relative to vehicle-treated control wells is depicted on the right ($n = 4$ biological replicates). **b**, **c**, Conditioned media (CM) was derived from drug-sensitive cells, treated with vehicle, vemurafenib or crizotinib. Drug-resistant cells were grown in this conditioned media and the cell number was determined on day 3. Drug-sensitive and drug-resistant cell lines and drugs used to generate

conditioned media as indicated. $n = 3$ (**b**) and 6 (**c**) biological replicates. **d**, Schematic diagram of the migration assay (top) and relative migration of A375^R cells towards conditioned media from different sources as indicated (bottom, $n = 10$ fields of vision (FOV)). **** $P < 0.0001$, two-tailed Mann-Whitney U test. **e**, Survival assay of drug-sensitive A375 cells cultured in conditioned media and treated with vemurafenib, assessed on day 3 ($n = 3$ biological replicates). **f**, Apoptosis rate of A375 cells cultured in conditioned media and treated with vemurafenib (3 μM) ($n = 3$ biological replicates). Data are mean and s.e.m.

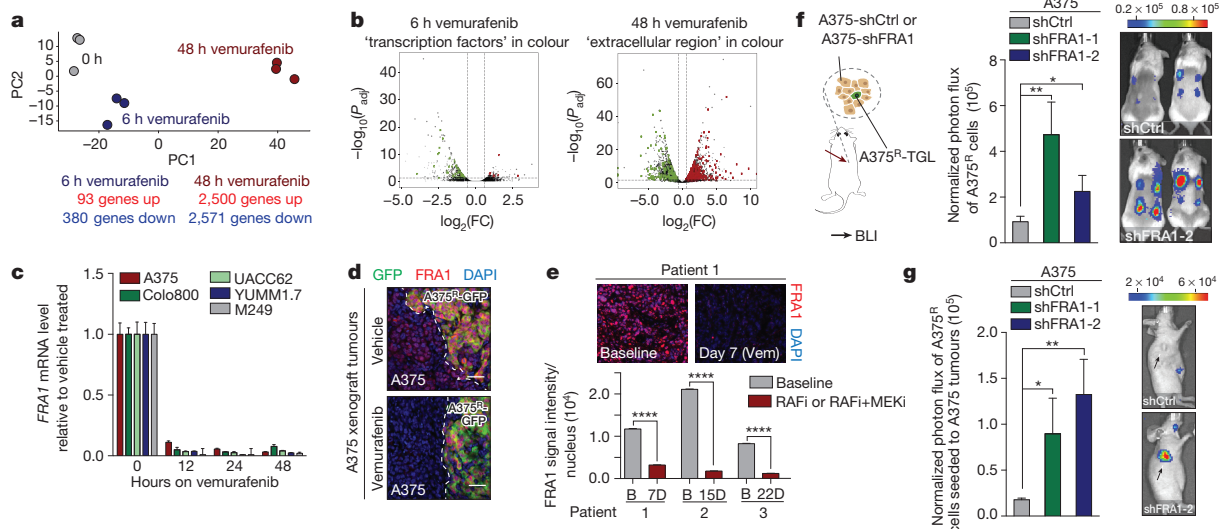


Figure 3 | FRA1 downregulation during RAFi treatment drives the reactive secretome. **a**, Principal component (PC) analysis of drug-sensitive A375 cells treated *in vitro* with vehicle or vemurafenib for 6 or 48 h. **b**, Volcano plots show genes significantly deregulated by vemurafenib treatment after 6 h (left) or 48 h (right). Transcription factors (TF) and gene products in the extracellular region are depicted in green (downregulated) and red (upregulated) ($n = 3$ tumours). P_{adj} , adjusted P value. **c**, Relative mRNA levels of *FRA1* during vemurafenib exposure [0.1–1 μM]. **d**, Representative immunofluorescence staining of A375/A375^R tumours for GFP (A375^R, green) and FRA1 (red) after vehicle or vemurafenib treatment (5 days). DAPI, 4',6-diamidino-2-phenylindole. Scale bars, 50 μm . **e**, Top, representative

immunofluorescence staining for FRA1 (red) of melanoma biopsy sections of patient 1. Original magnification, $\times 20$. Bottom, nuclear FRA1 staining was quantified in three melanoma patients before (B) and early-on therapy. RAFi and MEKi denote RAF and MEK inhibitors, respectively. **f**, Bioluminescent signal of A375^R-TGL cells 6 days after subcutaneous co-implantation with A375 cells expressing control (shCtrl) or two independent *FRA1* shRNAs (shFRA1-1 and shFRA1-2) ($n = 16$ tumours). **g**, Seeding of A375^R-TGL cells to unlabelled tumours expressing control or two independent shRNAs for *FRA1*, determined by BLI (vehicle, $n = 10$; shFRA1-1, $n = 10$; shFRA1-2, $n = 8$ tumours). Data are mean and s.e.m. * $P < 0.05$, ** $P < 0.01$, **** $P < 0.0001$, Student's t -test.

tumours *in vivo* after 5 days of vemurafenib treatment (Fig. 3a, b and Extended Data Fig. 3c). Similar extensive gene expression changes were observed in Colo800 and UACC62 melanoma cells treated with vemurafenib and H3122 lung adenocarcinoma cells treated with crizotinib (Extended Data Fig. 3d). Despite different cell lineages, different oncogenic drivers, and different targeted therapies we observed a significant overlap between the secretome of melanoma and lung adenocarcinoma cells ($P < 9.11 \times 10^{-5}$) (Extended Data Fig. 3e–h and Supplementary Table 1). Furthermore, changes in the secretome of vemurafenib-sensitive melanoma cells coincided with changes in the immune cell composition (Extended Data Fig. 4a, b), and with changes of soluble mediators derived from murine stromal cells such as IGF1 and HGF (Extended Data Fig. 4c, d). These data indicate a therapy-induced secretome (TIS), a response that consists of many up- and downregulated secreted factors, permeates the regressing tumour microenvironment and stimulates cancer cells, probably also stromal cells.

To identify molecular drivers of the A375-TIS in response to vemurafenib, we integrated the data of differentially expressed transcription factors after 6 h of vemurafenib treatment with the transcription factor binding motifs that were enriched at the promoters of differentially expressed genes in the secretome after 48 h (Fig. 3a, b). This analysis highlighted FRA1 (also known FOSL1), a member of the AP1 transcription factor complex and effector of the ERK pathway²⁷, as one of the putative upstream regulators of the TIS (Extended Data Fig. 5a). FRA1 was downregulated in all drug-sensitive cells, but not in resistant cells, treated with vemurafenib, crizotinib and erlotinib (Fig. 3c, d and Extended Data Fig. 5b–d). Biopsies from melanoma patients early during RAFi treatment confirmed RAFi-induced FRA1 downregulation in clinical samples (Fig. 3e, Extended Data Fig. 5e and Extended Data Table 1).

To test the functional role of FRA1 in modulating the TIS, we used RNA interference (RNAi) to inhibit FRA1 expression. Co-culture and conditioned media assays using A375 cells expressing short hairpin

RNAs targeting FRA1 (shFRA1) showed similar growth-accelerating and chemotactic activity on A375^R cells as vemurafenib treatment (Extended Data Fig. 6a–d). In line with these results, FRA1 knockdown in A375 cells induced transcriptional changes similar to those induced by vemurafenib (Extended Data Fig. 6e). A375^R cells co-implanted with A375 or UACC62 cells expressing shFRA1 also demonstrated increased growth *in vivo* (Fig. 3f and Extended Data Fig. 6f). A375-shFRA1 tumours attracted significantly more resistant cells from the circulation than tumours expressing the control vector (Fig. 3g). Thus, FRA1 downregulation drives the induction of the tumour-promoting secretome of vemurafenib-treated cancer cells.

To determine the effect of the reactive secretome on the drug-resistant tumour subpopulation in a regressing tumour, we expressed the ribosomal protein L10a (RPL10a) fused to enhanced green fluorescent protein (eGFP–RPL10a) in A375^R cells, allowing the specific retrieval of transcripts from A375^R cells by polysome immunoprecipitation for subsequent RNA-sequencing (RNA-seq) analysis²⁸ (Fig. 4a). In line with the *in vivo* phenotype of accelerated growth, the gene expression pattern of resistant cells in the regressing microenvironment was enriched for biological processes involved in cell viability, proliferation and cell movement (Extended Data Fig. 7a). Pathway analysis of the expression data suggested activation of several pathways including PI(3)K/AKT, BMP-SMAD and NFκB (Fig. 4b). The hyperactivity of the PI(3)K/AKT pathway in this context also suggested a potential vulnerability of the cells to PI(3)K/mTOR inhibitors (Extended Data Fig. 7b). The pathway-analysis-based prediction of PI(3)K/AKT activation was also reflected at the protein level in both resistant and sensitive cells in the presence of CM-vemurafenib *in vitro* and under vemurafenib treatment *in vivo* (Fig. 4c and Extended Data Fig. 7c, d). Moreover, PI(3)K/AKT emerged as the dominant TIS responsive pathway in a targeted immunoblot analysis of survival pathways *in vitro* (Extended Data Fig. 7e).

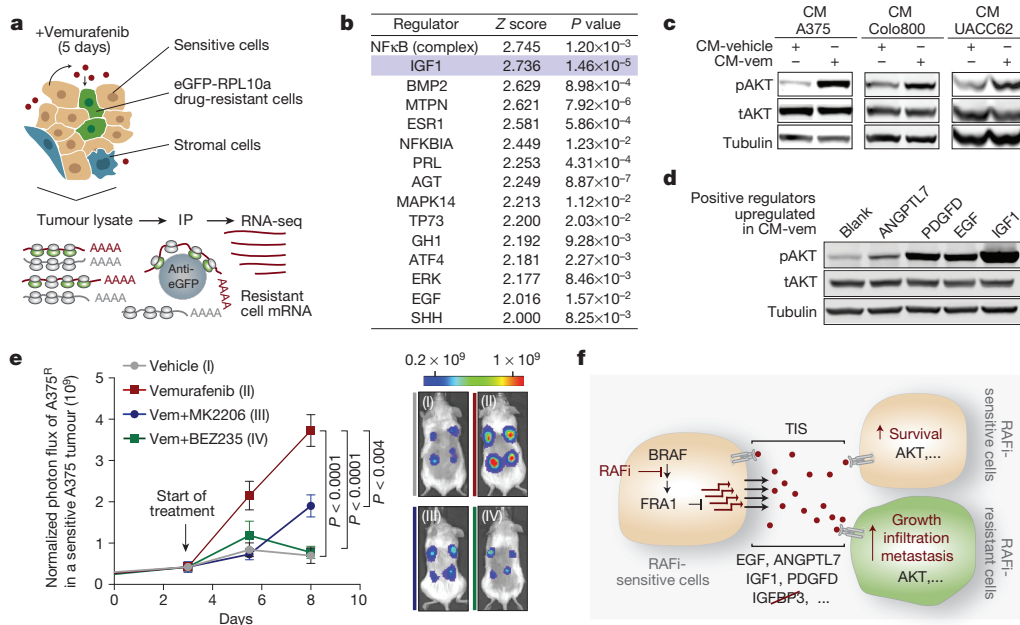


Figure 4 | The therapy-induced secretome in melanoma promotes relapse by activating the AKT pathway in resistant cells. **a**, Schematic diagram showing the isolation of polysome-associated transcripts from resistant cells by translating ribosome affinity profiling (TRAP) from tumours during treatment. IP, immunoprecipitation. **b**, Ingenuity upstream regulator analysis of gene expression profiles from A375^R cells responding to a regressing tumour microenvironment (5 days of treatment; $n = 3$ tumours). **c**, Phosphorylation status of AKT^{S473} (pAKT) in A375^R cells, stimulated for 15 min with various conditioned media, as indicated by immunoblotting. tAKT, total AKT. **d**, Phosphorylation status of AKT^{S473} in A375^R cells after stimulation with

positive regulators of the AKT pathway, upregulated in the melanoma TIS; ANGPTL7 ($5 \mu\text{g ml}^{-1}$, 30 min; upregulated in A375, Colo800, UACC62), PDGFD (10 ng ml^{-1} , 10 min; upregulated in Colo800), EGF (10 ng ml^{-1} , 10 min; upregulated in A375) and IGF1 (10 ng ml^{-1} , 10 min; upregulated in UACC62). **e**, Mice bearing A375/A375^R-TGL tumours were treated with drugs, and growth of A375^R cells was followed by BLI (vehicle, $n = 14$; vemurafenib, $n = 16$; vemurafenib and BEZ235, $n = 16$; vemurafenib and MK2206, $n = 8$ tumours). **f**, Graphical summary of the findings. Data are mean and s.e.m. P values calculated using a two-tailed Mann–Whitney U test.

The TIS contained many mediators directly or indirectly activating the AKT pathway. Positive mediators that were upregulated during therapy included IGF1, EGF, ANGPTL7 and PDGFD, each of which activated the AKT pathway *in vitro* (Fig. 4d). IGF1, one of the most potent activators of the AKT pathway, is also abundantly expressed in the tumour stroma and is further upregulated during targeted therapy (Extended Data Figs 4c and 7f). In addition, levels of IGF1, a negative regulator of IGF1, were markedly reduced in the TIS of all investigated cell lines, favouring increased AKT pathway activation in the presence of IGF1 and stimulation of proliferation of resistant cells *in vivo* (Extended Data Fig. 7f–k).

To test the role of AKT activation as a mediator of TIS-induced tumour proliferation, we combined vemurafenib with AKT/PI(3)K/mTOR inhibitors. In co-culture and proliferation experiments using conditioned media, dual inhibition of the MAPK and AKT pathway diminished the growth benefit of the TIS (Extended Data Fig. 8a, b). We then treated mice with A375/A375^R or A375^R tumours with vemurafenib and AKT (MK2206) or PI(3)K/mTOR inhibitors (BEZ235). The combined inhibition of MAPK and PI(3)K/AKT/mTOR pathways significantly blunted the outgrowth of vemurafenib-resistant cells in the A375/A375^R tumours (Fig. 4e). The growth inhibition was specific for the amplified proliferation in the regressing tumour microenvironment and had no effects on the growth of resistant cells alone (Extended Data Fig. 8c). Furthermore, the outgrowth of resistant A375^R cells in tumour seeding assays was significantly reduced when regressing tumours were co-treated with BEZ235 (Extended Data Fig. 8d). Thus, the TIS-induced proliferation is susceptible to therapeutic targeting.

The limited effectiveness of targeted therapies has been attributed to intracellular feedback loops and specific cytokines that support the survival of drug-sensitive cells. From these residual tumours, clones emerge that are intrinsically resistant to targeted therapy and are ultimately responsible for clinical relapse. Our work demonstrates that targeted inhibition of a cancer driver pathway can paradoxically promote these two aspects of drug resistance via induction of a complex, reactive secretome. This TIS not only enhances the survival of drug-sensitive cells, but also acutely accelerates the expansion and dissemination of drug-resistant clones. Rather than a cell death by-product^{29,30}, the TIS is a live-cell response to inhibition of an oncogenic driver pathway, mediated by a concrete transcriptional program, and defined by specific alterations of intracellular signalling networks (Fig. 4f).

Our identification of AKT signalling as a mediator of TIS-induced tumour progression in BRAF-driven melanoma is in line with AKT activation in tumours observed in the clinic during vemurafenib treatment¹⁶. Patients treated with BRAF inhibitor rarely show full tumour regression^{3,4}, and the remaining drug-responsive tumour cells may remain a source of TIS for the duration of the treatment. Our results provide a rationale for combining PI(3)K/AKT/mTOR pathway inhibitors with inhibitors of the MAPK pathway in the treatment of these tumours. However, the breadth of the TIS and the generality of our findings across different cell lineages, drugs (vemurafenib, crizotinib and erlotinib), and resistance mechanisms suggest that durable responses may require the combination of this type of agents with a radically different therapeutic modality.

Online Content Methods, along with any additional Extended Data display items and Source Data, are available in the online version of the paper; references unique to these sections appear only in the online paper.

Received 26 August 2014; accepted 12 February 2015.

Published online 25 March 2015.

- Engelman, J. A. & Settleman, J. Acquired resistance to tyrosine kinase inhibitors during cancer therapy. *Curr. Opin. Genet. Dev.* **18**, 73–79 (2008).
- Holohan, C., Van Schaeybroeck, S., Longley, D. B. & Johnston, P. G. Cancer drug resistance: an evolving paradigm. *Nature Rev. Cancer* **13**, 714–726 (2013).
- Chapman, P. B. *et al.* Improved survival with vemurafenib in melanoma with BRAF V600E mutation. *N. Engl. J. Med.* **364**, 2507–2516 (2011).

- Sosman, J. A. *et al.* Survival in BRAF V600-mutant advanced melanoma treated with vemurafenib. *N. Engl. J. Med.* **366**, 707–714 (2012).
- Shaw, A. T. & Engelman, J. A. ALK in lung cancer: past, present, and future. *J. Clin. Oncol.* **31**, 1105–1111 (2013).
- Zhou, C. *et al.* Erlotinib versus chemotherapy as first-line treatment for patients with advanced EGFR mutation-positive non-small-cell lung cancer (OPTIMAL, CTONG-0802): a multicentre, open-label, randomised, phase 3 study. *Lancet Oncol.* **12**, 735–742 (2011).
- Villanueva, J. *et al.* Acquired resistance to BRAF inhibitors mediated by a RAF kinase switch in melanoma can be overcome by cotargeting MEK and IGF-1R/PI3K. *Cancer Cell* **18**, 683–695 (2010).
- Nazarian, R. *et al.* Melanomas acquire resistance to B-RAF(V600E) inhibition by RTK or N-RAS upregulation. *Nature* **468**, 973–977 (2010).
- Poulikakos, P. I. *et al.* RAF inhibitor resistance is mediated by dimerization of aberrantly spliced BRAF(V600E). *Nature* **480**, 387–390 (2011).
- Wagle, N. *et al.* Dissecting therapeutic resistance to RAF inhibition in melanoma by tumor genomic profiling. *J. Clin. Oncol.* **29**, 3085–3096 (2011).
- Lito, P. *et al.* Relief of profound feedback inhibition of mitogenic signaling by RAF inhibitors attenuates their activity in BRAFV600E melanomas. *Cancer Cell* **22**, 668–682 (2012).
- Shi, H. *et al.* Melanoma whole-exome sequencing identifies V600EB-RAF amplification-mediated acquired B-RAF inhibitor resistance. *Nature Commun.* **3**, 724–728 (2012).
- Wilson, T. R. *et al.* Widespread potential for growth-factor-driven resistance to anticancer kinase inhibitors. *Nature* **487**, 505–509 (2012).
- Straussman, R. *et al.* Tumour micro-environment elicits innate resistance to RAF inhibitors through HGF secretion. *Nature* **487**, 500–504 (2012).
- Johannessen, C. M. *et al.* A melanocyte lineage program confers resistance to MAP kinase pathway inhibition. *Nature* **504**, 138–142 (2013).
- Shi, H. *et al.* A novel AKT1 mutant amplifies an adaptive melanoma response to BRAF inhibition. *Cancer Discovery* **4**, 69–79 (2014).
- Diaz, L. A. Jr *et al.* The molecular evolution of acquired resistance to targeted EGFR blockade in colorectal cancers. *Nature* **486**, 537–540 (2012).
- Shi, H. *et al.* Acquired resistance and clonal evolution in melanoma during BRAF inhibitor therapy. *Cancer Discovery* **4**, 80–93 (2014).
- Sharma, S. V. *et al.* A chromatin-mediated reversible drug-tolerant state in cancer cell subpopulations. *Cell* **141**, 69–80 (2010).
- Kim, M. Y. *et al.* Tumor self-seeding by circulating cancer cells. *Cell* **139**, 1315–1326 (2009).
- Villanueva, J. & Herlyn, M. Melanoma and the tumor microenvironment. *Curr. Oncol. Rep.* **10**, 439–446 (2008).
- Acharyya, S. *et al.* A CXCL1 paracrine network links cancer chemoresistance and metastasis. *Cell* **150**, 165–178 (2012).
- Sun, Y. *et al.* Treatment-induced damage to the tumor microenvironment promotes prostate cancer therapy resistance through WNT16B. *Nature Med.* **18**, 1359–1368 (2012).
- Lee, H. J. *et al.* Drug resistance via feedback activation of Stat3 in oncogene-addicted cancer cells. *Cancer Cell* **26**, 207–221 (2014).
- Lito, P., Rosen, N. & Solit, D. B. Tumor adaptation and resistance to RAF inhibitors. *Nature Med.* **19**, 1401–1409 (2013).
- Sun, C. *et al.* Reversible and adaptive resistance to BRAF(V600E) inhibition in melanoma. *Nature* **508**, 118–122 (2014).
- Joseph, E. W. *et al.* The RAF inhibitor PLX4032 inhibits ERK signaling and tumor cell proliferation in a V600E BRAF-selective manner. *Proc. Natl Acad. Sci. USA* **107**, 14903–14908 (2010).
- Heiman, M. *et al.* A translational profiling approach for the molecular characterization of CNS cell types. *Cell* **135**, 738–748 (2008).
- Fuchs, Y. & Steller, H. Programmed cell death in animal development and disease. *Cell* **147**, 742–758 (2011).
- Kurtova, A. V. *et al.* Blocking PGE₂-induced tumour repopulation abrogates bladder cancer chemoresistance. *Nature* **517**, 209–213 (2015).

Supplementary Information is available in the online version of the paper.

Acknowledgements We thank members of the Massagué laboratory for discussions; L. Sevenich and L. Akkari for technical advice. This work was supported by grants from the AACR (SU2C) to R.S.L., the MSK Metastasis Research Center, the NIH (CA163167 and CA129243), the Congressionally Directed Medical Research Program of the Department of Defense, the Howard Hughes Medical Institute, and the Cancer Center Support Grant P30 CA008748 to J.M., A.C.O. was an Erwin Schrodinger Fellowship awardee (J3013, FWF, Austrian Science Fund). A.L.J. was a Medical Research Fellow of the Howard Hughes Medical Institute. S.V. is supported by the Medical Research Council.

Author contributions A.C.O. and J.M. conceived the project, designed the experiments and wrote the paper. A.C.O. performed experiments and computational analysis. A.L.J., Y.Z., W.S. and T.W. assisted with experiments. Y.Z. and S.V. performed computational analysis. M.C.B. provided cell lines. X.K., H.S. and R.S.L. provided patient samples. N.R. provided clinical expertise, cell lines and drugs. All authors interpreted data, discussed results, and revised the manuscript.

Author Information All RNA-seq data has been deposited in the Gene Expression Omnibus database under accession number GSE64741. Reprints and permissions information is available at www.nature.com/reprints. The authors declare no competing financial interests. Readers are welcome to comment on the online version of the paper. Correspondence and requests for materials should be addressed to J.M. (j-massague@ski.mskcc.org).

METHODS

Cell culture. A375, M249 (ref. 8) and B16 cells were cultured in DMEM media; Colo800, UACC62, SKMEL239-clone3, LOX, PC9, H2030, H3122 and HCC827 cells were cultured in RPMI media. YUMM1.1 and YUMM1.7 were cultured in DMEM/F12 media. GPG29 and 293T cells were used for retrovirus and lentivirus production, respectively. Both were maintained in DMEM media. All media contained 10% FBS, 2 mM L-glutamine, 100 IU ml⁻¹ penicillin/streptomycin and 1 µg ml⁻¹ amphotericin B, the media for GPG29 contained in addition 0.3 mg ml⁻¹ G418, 20 ng ml⁻¹ doxycycline and 2 µg ml⁻¹ puromycin. All cells were grown in a humidified incubator at 37 °C with 5% CO₂ and were tested regularly for mycoplasma contamination. All cell lines used were negative for mycoplasma.

To generate vemurafenib-resistant melanoma cell lines, vemurafenib-sensitive cell lines were seeded at low density and exposed to 1–3 µM vemurafenib (LC-Labs). After approximately 8 weeks of continuous vemurafenib exposure, we derived resistant cell clones that were maintained on vemurafenib (1 µM vemurafenib for M249^{R4}, Colo800^R, LOX^R, UACC62^R; 2 µM vemurafenib for A375^R, YUMM1.7^R). The same protocol was performed to generate a crizotinib-resistant cell line from H3122 lung adenocarcinoma cells, which were selected and maintained with 300 nM crizotinib. Drug-sensitive and resistant melanoma cell lines from A375, Colo800, UACC62 and YUMM1.7 and the drug sensitive lung adenocarcinoma cell lines H3122 and HCC827 were exposed to increasing doses of vemurafenib and the number of cells was determined after 3 days and pERK levels after 1 h of vemurafenib, crizotinib or erlotinib exposure (Extended Data Fig. 9a–j). Receptor status was determined by western blot and showed an increase in EGFR expression levels in all resistant lines examined as well as an increase in MET receptor expression in A375^R and UACC62^R cells compared to their parental, drug-sensitive cells (Extended Data Fig. 9k).

For co-culture assays sensitive cells were plated in 12-well or 24-well plates and allowed to adhere overnight in regular growth media. Media was then replaced with low serum (2% FBS) media containing vehicle, 0.1 µM vemurafenib, 0.3 µM crizotinib or 0.01 µM erlotinib. For control wells media containing vehicle or 0.1 µM vemurafenib, 0.3 µM crizotinib, or 0.01 µM erlotinib was plated at the same time. After 48 h, TGL-expressing, resistant cells were plated on top of the vehicle/drug treated cells or in media-only control wells. Media containing vehicle/drug was replenished every 48 h. After 7 days, luciferin [150 µg ml⁻¹] was added to the wells and luciferase-signal of resistant cells was determined by BLI using a Xenogen Spectrum imaging machine (Perkin Elmer). Co-culture experiments were independently performed at least twice and a representative experiment is shown.

To generate conditioned media, 2.3 × 10⁶ and 6.4 × 10⁶ drug-sensitive cells were plated on 15-cm dishes in regular growth media and allowed to adhere overnight. The media was then replaced by low serum media containing vehicle or vemurafenib (0.1 µM for A375 cells, 1 µM for all other cell lines), on dishes containing 2.3 × 10⁶ and 6.4 × 10⁶ drug-sensitive cells, respectively. The same procedure was followed for generation of conditioned media from H3122 (crizotinib, 0.3 or 1 µM) or HCC827 (erlotinib 0.01 µM) lung adenocarcinoma cells. After 72 h, cells on both plates had reached equal confluency of ~80% and conditioned media was collected, centrifuged at 1,000 r.p.m. for 5 min, filtered, and aliquots were stored at –80 °C until further use. Key proliferation and migration experiments yielded the same results when performed with conditioned media in which the same number of drug-sensitive cells (3.2 × 10⁶) was plated initially, which resulted in higher cell confluency in the vehicle-treated dish at time of conditioned media collection.

Proliferation, survival and apoptosis assays. Around 1,000–3,000 cells were plated in a 96-well plate, allowed to adhere overnight, and then incubated with either fresh or conditioned media containing vemurafenib or additional drugs as indicated. After 72 h, the number of cells was determined using a CelltiterGlo assay and the caspase 3/7 activity using a CaspaseGlo assay (Promega) according to the manufacturer's instructions. Caspase 3/7 activity was normalized to the number of cells present. All experiments with melanoma test cells and melanoma conditioned media were performed at least three times, experiments with lung adenocarcinoma cell lines were performed at least twice. Representative experiments are shown.

Boyden chamber transwell migration assay/gap closure assay. Transwell migration assays were performed as described previously with minor modifications³¹. In brief, serum-starved cells (0.2% FBS, overnight) were labelled with cell tracker green (Invitrogen) for 30 min at 37 °C and allowed to recover for 1 h. Cells (25,000–50,000) were then seeded onto membrane inserts with 8-µm pores and fluorescence blocking filters (Falcon). The number of cells migrated through the pores of the membrane was scored after 5–24 h using an Evos microscope (AMG). Gap closing assay was performed according to standard protocols. In brief, cells were seeded and grown until confluent. A tip was used to generate a gap, cells were washed and conditioned media was added. Images were acquired over time to monitor for gap closure in different conditions. All experiments were performed independently at least twice. Representative experiments are shown.

xCELLigence migration assay. Experiments were performed using the xCELLigence RTCA DP instrument (Roche Diagnostics GmbH) placed in a humidified incubator at 37 °C with 5% CO₂. Cell migration experiments were performed using modified 16-well plates (CIM-16, Roche Diagnostics GmbH) according to the manufacturer's instructions. The experiment was performed twice. A representative experiment is shown.

Animal studies. All experiments using animals were performed in accordance to our protocol approved by MSKCC's Institutional Animal Care and Use Committee (IACUC). 5–7-week-old, female NOD-SCID NCR (NCI) or athymic NCR-NU-NU (NCI) mice were used for animal experiments with human cell lines. Primary YUMM1.1 and YUMM1.7 cell lines were isolated from melanomas developed in mice (*Tyr::CreER; Braf^{CA}; Cdkn2a^{-/-} Pten^{lox/lox}*) treated with 4-hydroxytamoxifen and were subsequently implanted in female C57BL/6J (JAX) mice aged between 5 and 7 weeks. Tumour formation, outgrowth and metastasis were monitored by BLI of TGL-labelled tumour cells as described previously²². In brief, anaesthetized mice (150 mg kg⁻¹ ketamine, 15 mg kg⁻¹ xylazine or isoflurane) were injected retro-orbitally with D-luciferin (150 mg kg⁻¹) and imaged with an IVIS Spectrum Xenogen machine (Caliper Life Sciences). Bioluminescence analysis was performed using Living Image software, version 4.4. For co-implantation assays, mice were anaesthetized (150 mg kg⁻¹ ketamine, 15 mg kg⁻¹ xylazine) and 1 × 10³ TGL-labelled resistant tumour cells were injected subcutaneously with 2 × 10⁶ sensitive tumour cells in 50 µl growth-factor-reduced Matrigel/PBS (1:1) (BD Biosciences). For the control groups in which the effects of drug treatment on resistant cells alone were tested, 2 × 10⁶ resistant cells were injected in growth-factor-reduced Matrigel/PBS. Two-to-four sites on the flanks were injected per mouse. After tumours reached a size of 50–150 mm³, the BLI signal of resistant cells was determined. To compensate for minor growth differences of the GFP⁺ resistant cell population between mice, the mice were assigned to the cohorts so that the overall BLI intensity (and consequently the cell number) was equal in the treatment and control group. Each group received vehicle or drug treatment as indicated (vemurafenib/PLX4032, 25 mg kg⁻¹ twice daily for YUMM1.1 and YUMM1.7 tumours, and 75 mg kg⁻¹ twice daily for all other BRAF mutant tumours, LC-Labs or Selleckchem; 100 mg kg⁻¹ crizotinib once daily, LC-Labs; 50 mg kg⁻¹ erlotinib once daily, LC-Labs; 100 mg kg⁻¹ MK-2206 once daily, Chemietek; 50 mg kg⁻¹ BEZ235 once daily, LC-Labs). Growth of the resistant population in the different groups was monitored by BLI, quantified and normalized to BLI signal at start of treatment. Tumour seeding and metastasis assays were performed as described with minor modifications²⁰. In brief, sensitive tumour cells were injected subcutaneously on two sites per mouse. Once tumours were established (50–150 mm³) mice were treated with vehicle or vemurafenib (75 mg kg⁻¹ twice daily) for 3 days, and 1 × 10⁵ TGL-labelled drug-resistant cells were injected in the left cardiac ventricle. Treatment was continued, and metastatic burden and tumour seeding were determined *in vivo* and *ex vivo* by BLI. Tumour volume was determined using caliper measurements and calculated using the following formula: tumour volume = (D × d²)/2, in which D and d refer to the long and short tumour diameter, respectively. All experiments with A375 cells were independently performed at least three times, except animal experiments in Fig. 3, which were performed twice. All other animal experiments were independently performed at least twice. Representative experiments are shown, except where noted and where instead the average of three experiments is presented.

Gene expression analysis. Whole RNA was isolated from cells using RNAeasy Mini Kit (QIAGEN). The Transcriptor First Strand cDNA synthesis kit (Roche) was used to generate cDNA. Differential RNA levels were assessed using Taqman gene expression assays (Life technologies). Assays used for human genes are: Hs04187685, Hs00365742, Hs00605382, Hs00601975, Hs01099999, Hs00959010, Hs01029057, Hs00234244, Hs00905117, Hs00180842, Hs00989373, Hs00234140, Hs00195591, Hs00207691, Hs99999141, Hs01117294, Mm00607939, Mm99999915 and Mm04207958. Relative gene expression was normalized to internal control genes: *B2M* (Hs99999907_m1), *GAPDH* (Hs99999905_m1) and *ACTB* (Mm00607939_s1). Quantitative PCR reactions were performed on a ViiA7 Real-Time PCR system and analysed using ViiA7 software (Life Technologies). All data points represent at least four technical replicates and experiments were performed independently three times. A representative experiment is shown.

Cancer-cell-specific TRAP and sequencing. To investigate the gene expression changes specifically of drug-sensitive tumours during vemurafenib treatment, or gene expression changes of resistant cells exposed to a regressing tumour microenvironment, A375 and A375^R cells, respectively, were modified to express eGFP-RPL10a. Tumours derived from implanted A375-eGFP-RPL10a and A375^R-eGFP-RPL10a cells were homogenized and processed with the TRAP protocol as previously described^{28,32,33} with the following modifications: fresh tumour was homogenized with a Model PRO 200 homogenizer at speed 5 for four cycles of 15 s, RNasin Plus RNase inhibitor (Promega, N2615) was used as RNase inhibitor, and anti-eGFP antibody coated sepharose beads (GE Healthcare) were used for immunoprecipitation. Polysome-associated RNA was purified with RNAaqueous micro kit (Life

Technologies, AM1931). Ribogreen and the Agilent BioAnalyzer technologies were used to quantify and control the quality of RNA; 500 ng RNA (RNA integrity number (RIN) > 8.5) from each sample was used for library construction with TruSeq RNA Sample Prep Kit v2 (Illumina) according to the manufacturer's instructions. The samples were barcoded and run on a HiSeq 2000 platform in a 50-base-pair (bp)/50-bp or 75-bp/75-bp paired-end run, using the TruSeq SBS Kit v3 (Illumina). An average of 40 million paired reads was generated per sample.

RNA-seq analysis. For drug-sensitive A375, Colo800, UACC63 and H3122 cells, *in vitro*, raw paired-end sequencing reads were mapped to the human genome (build hg19) with STAR2.3.0e (ref. 34) using standard options. Uniquely mapped reads were counted for each gene using HTSeq v0.5.4 (ref. 35) with default settings. Read counts of each sample were normalized by library size using the 'DESeq' package of Bioconductor. Differential gene expression analysis between any two conditions was performed based on a model using the negative binomial distribution³⁵. Genes with false discovery rate (FDR) < 0.05, fold change larger than 1.5 or smaller than 0.667-fold, and average read counts larger than 10 were treated as differentially expressed genes. RNA-seq data from *in vivo* xenograft TRAP samples were processed with the following modifications to avoid potential mRNA contamination from host mouse tissue: raw sequencing reads were mapped to a hybrid genome consisting indexes of both human (build hg19) and mouse (build mm9) genomes. Only reads that uniquely mapped to human genome indexes were preserved and counted using HTSeq v0.5.4 (ref. 35).

Bioinformatics analysis. Heatmap visualization of data matrices was performed using the 'gplots' package of R. Principle component analysis of RNA-seq results was performed with the variance stabilizing transformation methods in 'DESeq' package of Bioconductor and the first two principal components were plotted. Volcano plots were derived from 'DESeq'-based differential gene expression analysis. Differentially expressed genes with transcription factor activity (GO:00037000) at 6 h of vemurafenib treatment and gene products located in the extracellular region (GO:0005576) at 48 h of vemurafenib treatment were identified using the Database for Annotation, Visualization and Integrated Discovery (DAVID)³⁶ v6.7 (<http://david.abcc.ncifcrf.gov/>) and enriched GO terms were visualized using REVIGO³⁷ (<http://revigo.irb.hr>). Enriched transcriptional regulators for the list of differentially expressed gene products in the extracellular region were predicted with DAVID v6.7 and this list compared to the gene expression levels of transcription factors after 6 h of vemurafenib treatment in A375 cells. Upstream regulators, functions associated with the gene expression profile and potential drug vulnerabilities were determined by interpenetrative phenomenological analysis (IPA) analysis on differentially expressed genes from A375^R-eGFP-RPL10a cells in different tumour microenvironments *in vivo*.

Immunoblotting. RIPA buffer (Cell Signaling) was used for cell lysis, according to the manufacturer's instructions, and the protein concentrations were determined by BCA Protein Assay kit (Pierce). Proteins were separated by SDS-PAGE using Bis-Tris 4–12% gradient polyacrylamide gels in the MOPS buffer system (Invitrogen) and transferred to nitrocellulose membranes (BioRad) according to standard protocols. Membranes were immunoblotted with antibodies against pERK^{T202/Y204} (4370), tERK (4696), pAKT^{S473} (4060), pAKT^{T308} (4056), tAKT (2920), EGFR (4267), MET (8198), PDGFRb (3169), pFRA1 (3880), caspase3 (9662), pPRAS40^{T246} (13175), p70S6K^{T389} (9205), pFAK^{Y397} (3283), pPKC^{betaIIS660} (9371), pNFkB^{S536} (3033), pβ-Catenin^{S33/37/T41} (9561), pSTAT-3^{Y705} (9145), pSTAT-5^{C11C5} (9359), pGSK3α/β^{S21/9} (9327), pCREB^{S133}/pATF-1 (9196) (Cell Signaling, 1:1,000), FRA1 (sc-605, Santa Cruz Biotechnology, 1:200) and tubulin (T6074, Sigma-Aldrich, 1:5,000) in Odyssey blocking buffer (LI-COR). After primary antibody incubation, membranes were probed with IRDye 800CW donkey-anti-mouse IgG (LI-COR) or IRDye 680RD goat-anti-rabbit IgG (LI-COR) secondary antibody (1:20,000) and imaged using the LI-COR Odyssey system. All immunoblots were performed independently at least twice. Tubulin served as a loading control.

Plasmids, recombinant protein and ELISA. Identifiers for shRNAs used in this study are: V3LHS-644610 (shFRA1-1), V3LHS-644611 (shFRA1-2), V3LHS-320021 (shIGFBP3-1) and V2LHS-111629 (shIGFBP3-2) (Dharmacon, GE Lifesciences). IGFBP3 ELISA (Raybiotech) was performed according to the manufacturer's instructions with 50 µg tumour lysate and conditioned media was diluted 1:5. Recombinant proteins were used at the following conditions: 10 ng ml⁻¹ IGF1 (Invitrogen), 10 ng ml⁻¹ EGF (Invitrogen), 10 ng ml⁻¹ PDGFD (R&D Systems), 2 µg ml⁻¹ IGFBP3 (Prospec) for 15 min, or 5 µg ml⁻¹ ANGPTL7 (R&D Systems) for 30 min.

Patient samples. Melanoma tissues were obtained from clinical trial patients or patients under standard clinical management with approval of the UCLA Institutional Review Board. Patient-informed consent was obtained for the research performed in this study.

Immunofluorescence. Tissues for BrdU-immunofluorescence staining were obtained after overnight fixation with 4% paraformaldehyde (PFA) at 4 °C, embedded in OCT compound (VWR) and stored at -80 °C. 10-µm thick cryosections on glass slides were used for immunofluorescence staining according to standard

protocols. Tissue for all other immunofluorescence experiments from xenograft tumours was obtained after fixation with 4% PFA at 4 °C and a series of dehydration steps from 15% to 30% sucrose, as described previously³⁸. In brief, tumours were sliced using a sliding microtome (Fisher). Tumour slices (80 µm) were blocked floating in 10% NGS, 2% BSA, 0.25% Triton in PBS for 2 h at room temperature. Primary antibodies were incubated overnight at 4 °C in the blocking solution and the next day for 30 min at room temperature. After washes in PBS-Triton 0.25%, secondary antibodies were added in the blocking solution and incubated for 2 h. After extensive washing in PBS-Triton 0.25%, nuclei were stained with Bis-Benzamide for 5 min at room temperature, tumour slices were washed and transferred to glass slides. Slices were mounted with ProLong Gold anti fade reagent (Invitrogen). Primary antibodies: GFP (GFP-1020, Aves Labs, 1:1,000), collagen IV (AP756, Millipore, 1:500), BrdU (ab6326, Abcam, 1:250), FRA1 (sc605, Santa Cruz, 1:200). Secondary antibodies: Alexa-Fluor-488 anti-chicken, Alexa-Fluor-555 anti-rabbit, Alexa-Fluor-555 anti-rat (Invitrogen). Stained sections were visualized using a Carl Zeiss Axioimager Z1 microscope or with a Leica SP5 upright confocal microscope using ×10 or ×20 objectives. Images were analysed with ImageJ, and Meta-morph software.

Flow cytometry. Flow cytometry was performed as described previously²², with minor modifications. In brief, whole tumours were dissected, cut into smaller sections and dissociated for 1–3 h with 0.5% collagenase type III (Worthington Biochemical) and 1% dispase II (Roche) in PBS. Resulting single cells suspensions were washed with PBS supplemented with 2% FBS and filtered through a 70-µm nylon mesh. The resulting single cell suspension was incubated for 10 min at 4 °C with anti-mouse Fc-block CD16/32 antibody (2.4G2 BD) in PBS supplemented with 1% BSA. Cells were subsequently washed with PBS/BSA and stained with control antibodies or antibodies to detect immune cells diluted in PBS supplemented with 0.5% BSA and 2 mM EDTA. The following antibodies against mouse antigens were used: CD45-PE-Cy7 (clone 30-F11, BD Pharmingen, 1:200), CD11b-APC (clone: M1/70, BD Pharmingen, 1:100), Gr1-PE (MACS, 1:10), CD31-APC (clone: 390, eBioscience, 1:100), F4/80-PE (clone: BM8, eBioscience, 1:50). To determine the level of EdU incorporation in A375^R cells within vehicle- or vemurafenib-treated A375/A375^R tumours, EdU (50 mg kg⁻¹, Life Technologies) was injected intraperitoneally, after 2 h tumours were collected, single-cell suspensions generated as described above and further processed according to the manufacturer's protocol (Click-iT Plus EdU Alexa Fluor 647 Flow Cytometry Assay Kit, Life technologies). Data were acquired using a FACS Calibur (BD Biosciences). All experiments were performed independently at least two times. Representative experiments are shown.

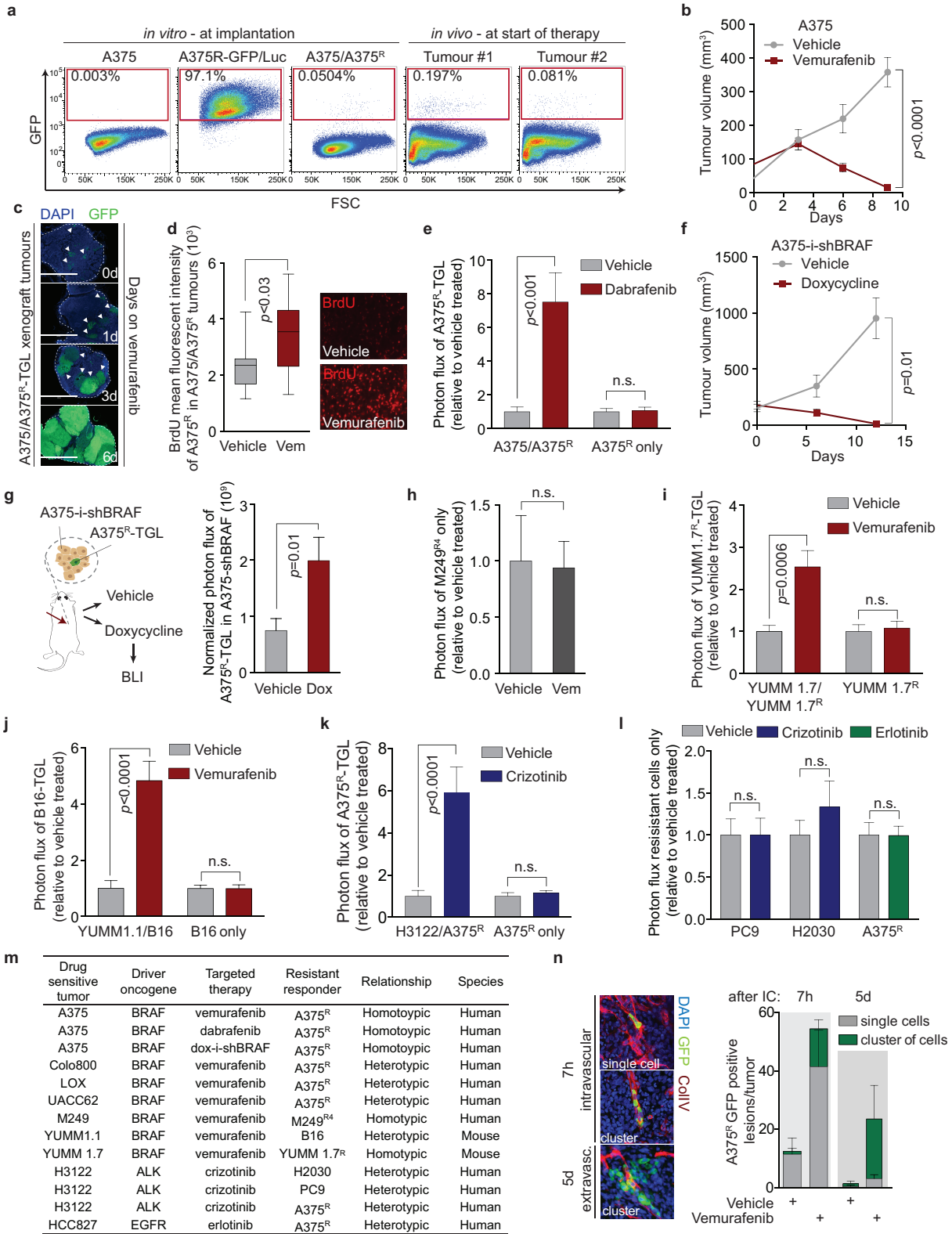
Antibody arrays. Cytokines and cytokine receptors of murine stromal and immune cells, in A375 tumours treated with vehicle or vemurafenib for 5 days, were measured using the Mouse Cytokine Array G2000 (RayBio, AAH-CYT-G2000-8, detecting 174 proteins), according to the recommended protocols. In brief, tumours were homogenized with a Mini Immersion Blender (Pro Scientific) in Raybio Lysis buffer with protease inhibitors. Lysates were centrifuged for 5 min at 10,000g, the supernatant was collected and protein concentration was measured using the BCA Assay Kit (Pierce). Protein (150 µg) was hybridized on the antibody arrays overnight at 4 °C. IRDye-labelled streptavidin (LI-COR) at a dilution of 1:5,000 was used for the detection, slides were scanned using a Odyssey CLx scanner (LI-COR) and analysed using Image Studio 2.0 software. The results were then normalized using internal controls, and the relative protein levels determined across four biological replicates.

Senescence β-galactosidase staining. A375 cells were grown in low-serum media and treated with vehicle or vemurafenib (0.1 µM) for 3 or 8 days, β-galactosidase staining was performed according to the manufacturer's instructions (Cell Signaling). All experiments were performed independently three times. Representative experiments are shown.

Statistical analysis. Data are generally expressed as mean ± s.e.m., or in box plots in which the centre line is the median, and whiskers are minimum to maximum values. Group sizes were determined based on the results of preliminary experiments and no statistical method was used to predetermine sample size. Group allocation and outcome assessment were not performed in a blinded manner. All samples that met proper experimental conditions were included in the analysis. Statistical significance was determined using a two-tailed Mann-Whitney *U* test or Student's *t*-test using Prism 6 software (GraphPad Software), or using a hypergeometric variability test (<http://www.geneprof.org>). Significance was set at *P* < 0.05.

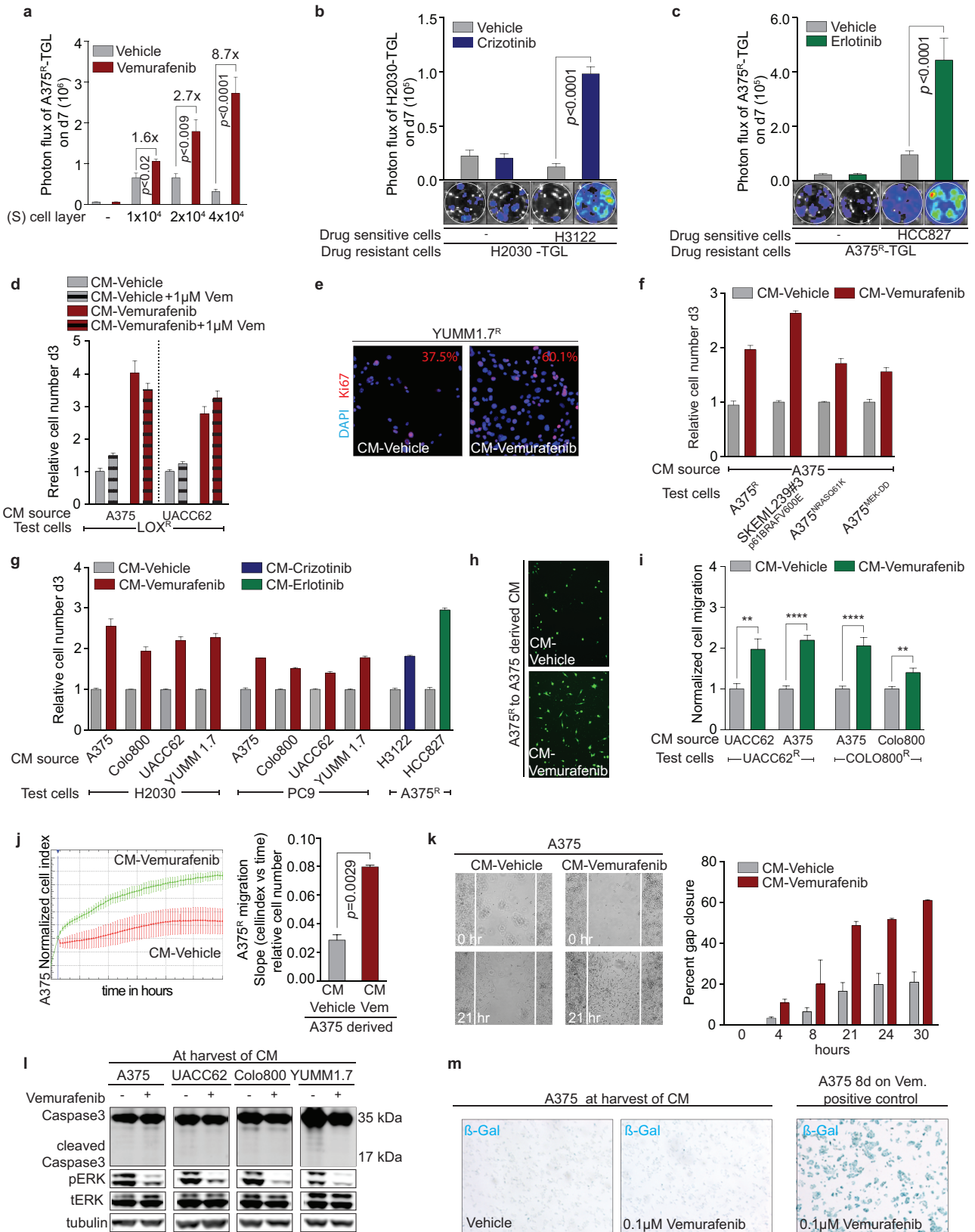
1. Tavazoie, S. F. *et al.* Endogenous human microRNAs that suppress breast cancer metastasis. *Nature* **451**, 147–152 (2008).
2. Doyle, J. P. *et al.* Application of a translational profiling approach for the comparative analysis of CNS cell types. *Cell* **135**, 749–762 (2008).
3. Zhang, X. H. *et al.* Selection of bone metastasis seeds by mesenchymal signals in the primary tumor stroma. *Cell* **154**, 1060–1073 (2013).
4. Dobin, A. *et al.* STAR: ultrafast universal RNA-seq aligner. *Bioinformatics* **29**, 15–21 (2013).

35. Anders, S. & Huber, W. Differential expression analysis for sequence count data. *Genome Biol.* **11**, R106 (2010).
36. Huang da, W., Sherman, B. T. & Lempicki, R. A. Systematic and integrative analysis of large gene lists using DAVID bioinformatics resources. *Nature Protocols* **4**, 44–57 (2009).
37. Supek, F., Bosnjak, M., Skunca, N. & Smuc, T. REVIGO summarizes and visualizes long lists of gene ontology terms. *PLoS ONE* **6**, e21800 (2011).
38. Valiente, M. *et al.* Serpins promote cancer cell survival and vascular co-option in brain metastasis. *Cell* **156**, 1002–1016 (2014).



Extended Data Figure 1 | Targeted therapy or oncogene knockdown leads to regression of sensitive melanoma and lung adenocarcinoma tumours but accelerates the proliferation and seeding of residual drug-resistant cells *in vivo*. **a**, FACS analysis of sensitive A375 and vemurafenib-resistant A375^R cells expressing TGL, at tumour implantation and after 2 weeks at start of therapy ($n = 8$ tumours). Plots depict representative images. **b**, Tumour volume of A375 cells treated with vehicle or vemurafenib over time (vehicle, $n = 8$; vemurafenib, $n = 12$ tumours). **c**, Representative sections of A375/A375^R-TGL tumours at 0, 1, 3 and 6 days of vemurafenib treatment analysed with immunofluorescence against GFP. Arrowheads indicate emerging clusters of GFP⁺ resistant cells. Scale bars, 2 mm. **d**, Quantification of BrdU incorporation into vemurafenib-resistant A375^R-TGL cells in A375/A375^R tumours treated with vehicle or vemurafenib for 6 days (vehicle, $n = 13$ FOV of 3 tumours; vemurafenib $n = 18$ FOV of 4 tumours). Original magnification, $\times 20$. **e**, Fold change of photon flux of TGL-expressing A375^R cells in A375 tumours or A375^R tumours alone treated with vehicle or dabrafenib for 8 days (A375/A375^R: vehicle, $n = 15$; dabrafenib, $n = 14$; A375^R: vehicle, $n = 8$; dabrafenib, $n = 7$ tumours). **f**, Tumour volume of doxycycline-inducible BRAF knockdown A375-i-shBRAF-derived xenograft tumours (in which 'A375-i' denotes expression of doxycycline-inducible hairpin) treated with vehicle or doxycycline over time (vehicle, $n = 5$; doxycycline, $n = 4$ tumours). **g**, Photon flux of TGL-expressing A375^R cells mixed in A375-i-shBRAF tumours treated with vehicle or doxycycline (vehicle, $n = 10$; doxycycline, $n = 11$ tumours). **h**, Fold change of photon flux of TGL-expressing vemurafenib-resistant M249^{R4} tumours treated with vehicle or vemurafenib ($n = 16$ tumours).

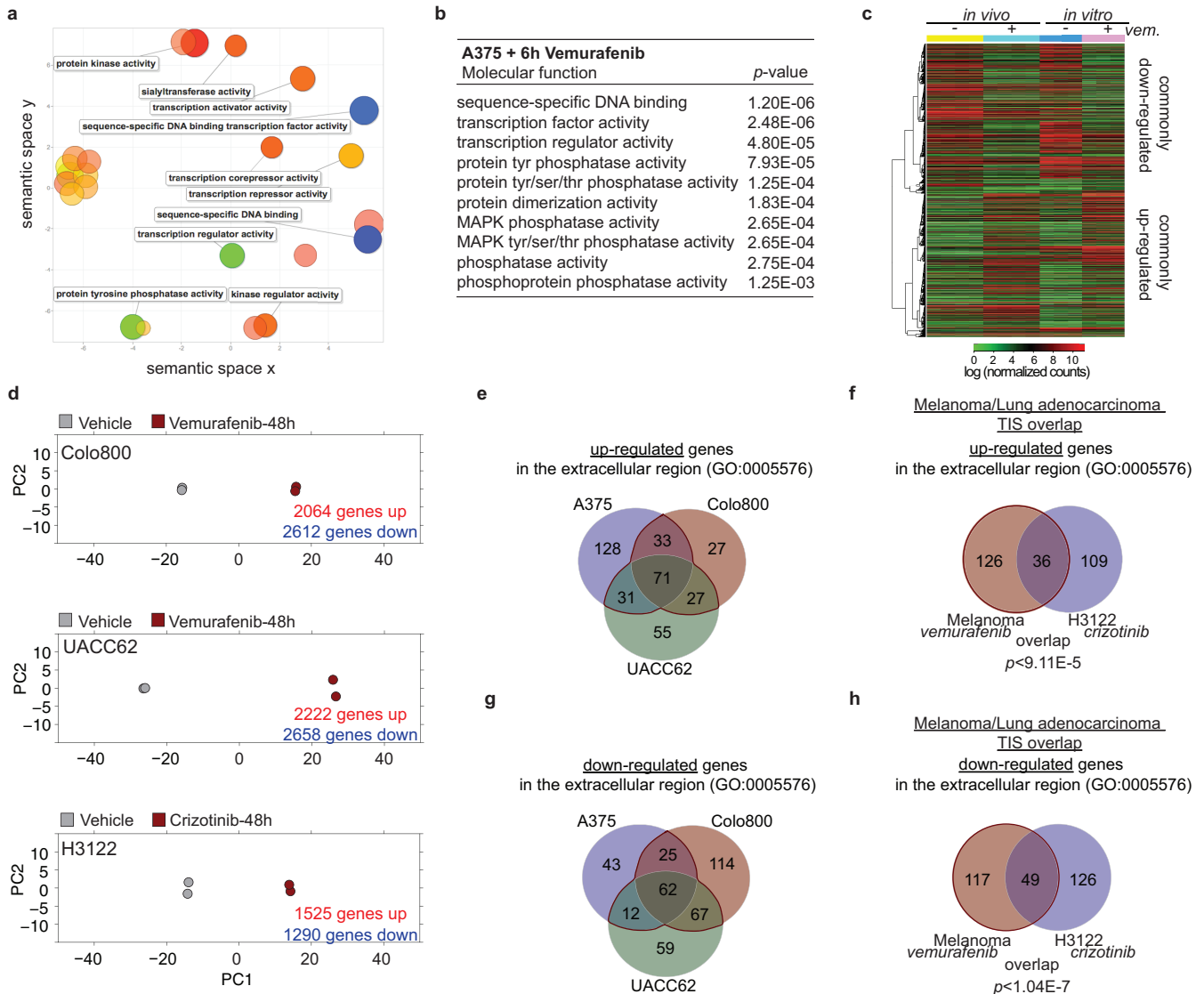
i–k, Co-implantation assay of tumours treated with vehicle or corresponding targeted therapy with BLI quantification after 5–8 days. **i**, Fold change of photon flux of TGL-expressing vemurafenib-resistant YUMM1.7^R cells mixed in unlabelled, vemurafenib-sensitive YUMM1.7 tumours or YUMM1.7^R tumours alone (YUMM1.7/YUMM1.7^R: $n = 24$; YUMM1.7^R: $n = 20$ tumours). **j**, Fold change of photon flux of TGL-expressing, intrinsically vemurafenib-resistant B16 cells mixed in vemurafenib-sensitive YUMM1.1 tumours or B16 tumours alone (YUMM1.1/B16: vehicle, $n = 12$; vemurafenib, $n = 16$; B16: $n = 20$ tumours). **k**, A375^R mixed in crizotinib-sensitive H3122 cells or A375^R tumours alone (H3122/A375^R: vehicle, $n = 14$; crizotinib, $n = 13$; A375^R: $n = 12$ tumours). **l**, Photon flux of tumours established from intrinsically resistant drug-resistant cells alone, treated with vehicle, crizotinib or erlotinib (crizotinib-resistant PC9, H2030- or erlotinib-resistant A375^R) (n (from left to right) = 12, 12, 7, 12, 16 and 16 tumours, respectively). **m**, Summary of the model systems and conditions used *in vivo*. **n**, Left, representative immunofluorescence images of vemurafenib-treated, sensitive tumours 7 h or 5 days after intracardiac injection with A375^R-TGL cells; sections stained for GFP (A375^R, green), collagen type IV (blood vessels, red), and DAPI (nuclei, blue). Right, quantification of A375^R single cells and cell clusters (≥ 2 cells) infiltrating an A375 tumour treated with vehicle or vemurafenib after intracardiac injection of A375^R cells (GFP⁺ cells were scored in at least 10 whole sections of at least 4 tumours). Original magnifications, $\times 20$. Data in **b**, **e–l** and **n** are mean and s.e.m., in **f**, centre line is median, whiskers are minimum to maximum. P values calculated by a two-tailed Mann–Whitney U test.



Extended Data Figure 2 | The secretome of vemurafenib-treated melanoma and crizotinib- or erlotinib-treated lung adenocarcinoma cells stimulates the proliferation and migration of drug-resistant cells *in vitro* and occurs before apoptosis and senescence.

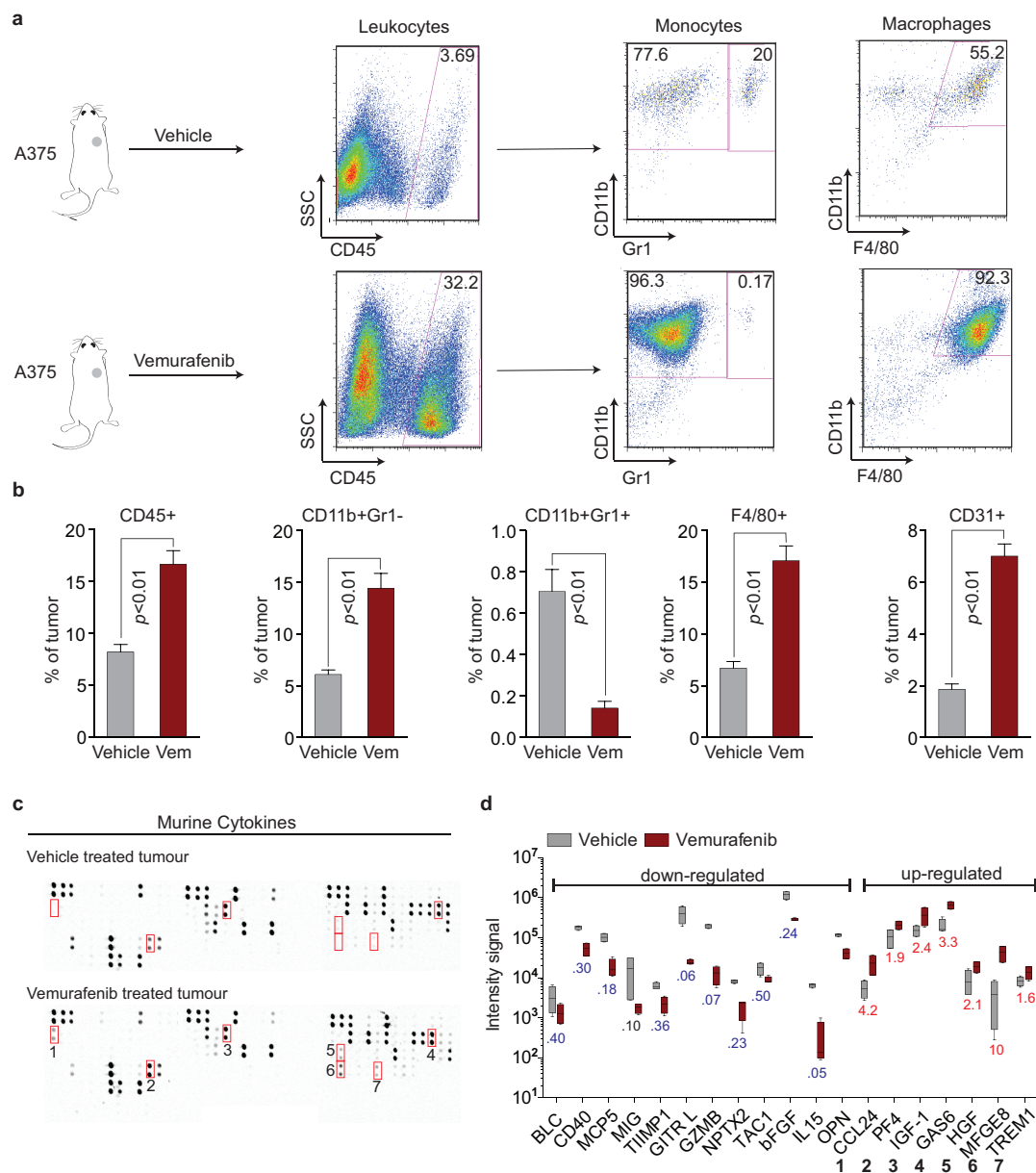
a, Quantification of the co-culture assay, depicted in Fig. 2a, 7 days after addition of resistant A375^R-TGL cells ($n = 4$ biological replicates). P values calculated using a Student's t -test. **b, c**, Drug-sensitive cells were pre-treated with vehicle or drug (crizotinib or erlotinib) for 48 h before 5×10^2 TGL-expressing, drug-resistant cells were added. Growth was monitored by BLI and quantified 7 days after addition of the resistant cell population ($n = 8$ biological replicates), P values calculated using a Student's t -test. **b**, Quantification and representative images of TGL-expressing H2030 cells alone or co-cultured with crizotinib-sensitive H3122 cells and treated with vehicle or crizotinib **c**, Quantification and representative images of TGL-expressing A375^R cells alone or co-cultured with erlotinib-sensitive HCC827 cells and treated with vehicle or erlotinib. **d**, Relative number of vemurafenib-resistant LOX^R cells after 3 days in the presence of conditioned media derived from A375 and UACC62 cells ($n = 3$ biological replicates). **e**, Representative immunofluorescence for Ki67 in drug-resistant YUMM1.7^R cells cultured in conditioned media from YUMM1.7 cells. Original magnification, $\times 20$. **f**, Relative number of vemurafenib-resistant melanoma cells with different, clinically relevant resistance mechanisms after 3 days in the presence of conditioned media derived from A375 cells. SKMEL239-3 expressing the p61 BRAFV600E splice variant, A375 expressing NRAS^{Q61K} or

the constitutively active MEK variant MEK-DD ($n = 5$ biological replicates). **g**, Relative cell number of intrinsically vemurafenib-resistant lung adenocarcinoma cells (H2030, PC9) or crizotinib- and erlotinib-resistant melanoma cells (A375^R) after 3 days cultured in the presence of conditioned media from vemurafenib-treated melanoma or crizotinib- and erlotinib-treated lung adenocarcinoma ($n = 6$ in all, except for A375^R with HCC827-CM, $n = 4$ biological replicates). **h**, Representative image of A375^R cells migrated towards A375-derived CM-vehicle or CM-vemurafenib. Original magnification, $\times 10$. **i**, Relative migration towards conditioned media from different sources and different resistant test cells as indicated ($n = 10$ FOV). $**P < 0.01$, $****P < 0.0001$, two-tailed Mann-Whitney U test. **j**, Representative graph and quantification of real-time migration of A375^R cells in the presence of conditioned media derived from A375 cells as measured by the xCELLigence system ($n = 4$ biological replicates). P value calculated using two-tailed Mann-Whitney U test. **k**, Monolayer gap closing assay of A375^R cells in the presence of conditioned media derived from A375 cells with representative light microscopy images and quantification of gap closure over time. **l**, Immunoblotting for cleaved caspase-3 and phosphorylated ERK protein levels in vemurafenib-sensitive melanoma cell lines after 72 h of vemurafenib treatment. **m**, β -galactosidase staining of A375 cells treated with vemurafenib for 72 h or 8 days. Original magnification, $\times 13$. Data are presented mean and s.e.m.



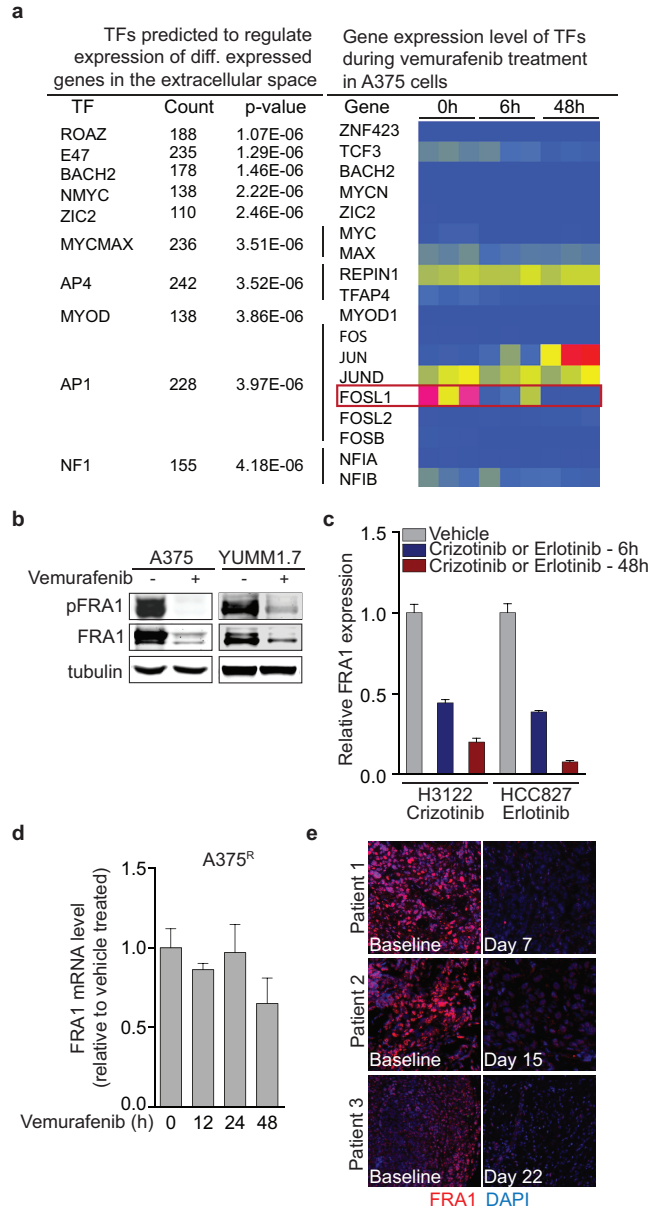
Extended Data Figure 3 | The therapy-induced secretome of sensitive cells overlaps significantly in melanoma and lung adenocarcinoma cells and appears after gene expression changes enriched for transcriptional regulators. **a, b**, GO analysis (<http://revigo.irb.hr>) of gene expression changes after 6 h of vemurafenib treatment of A375 cells with spatial representation of enriched GO terms (**a**) and the molecular functions significantly affected (**b**). **c**, Heat map representing the expression levels of commonly up- and downregulated genes in vemurafenib-treated A375-derived xenograft tumours (5 days) and A375 cells *in vitro* (48 h). **d**, Principal component analysis of vemurafenib-sensitive Colo800 and UACC62 melanoma cells and crizotinib-sensitive H3122 lung adenocarcinoma cells treated *in vitro* with vehicle or vemurafenib or crizotinib for 48 h. **e**, Venn diagram indicating the overlap of genes in the extracellular region (GO:0005576) upregulated after 48 h of

vemurafenib treatment in A375, Colo800 and UACC62 melanoma cell lines. **f**, Venn diagram indicating the overlap of genes in the extracellular region (GO:0005576) upregulated after 48 h of vemurafenib treatment in at least 2 out of 3 melanoma models and after 48 h of crizotinib treatment in the H3122 lung adenocarcinoma cell line. **g**, Venn diagram indicating the overlap of genes in the extracellular region (GO:0005576) downregulated after 48 h of vemurafenib treatment in A375, Colo800 and UACC62 melanoma cell lines. **h**, Venn diagram indicating the overlap of genes in the extracellular region (GO:0005576) downregulated after 48 h of vemurafenib treatment in at least 2 out of 3 melanoma models and after 48 h of crizotinib treatment in the H3122 lung adenocarcinoma cell line. *P* values calculated using a hypergeometric probability test.



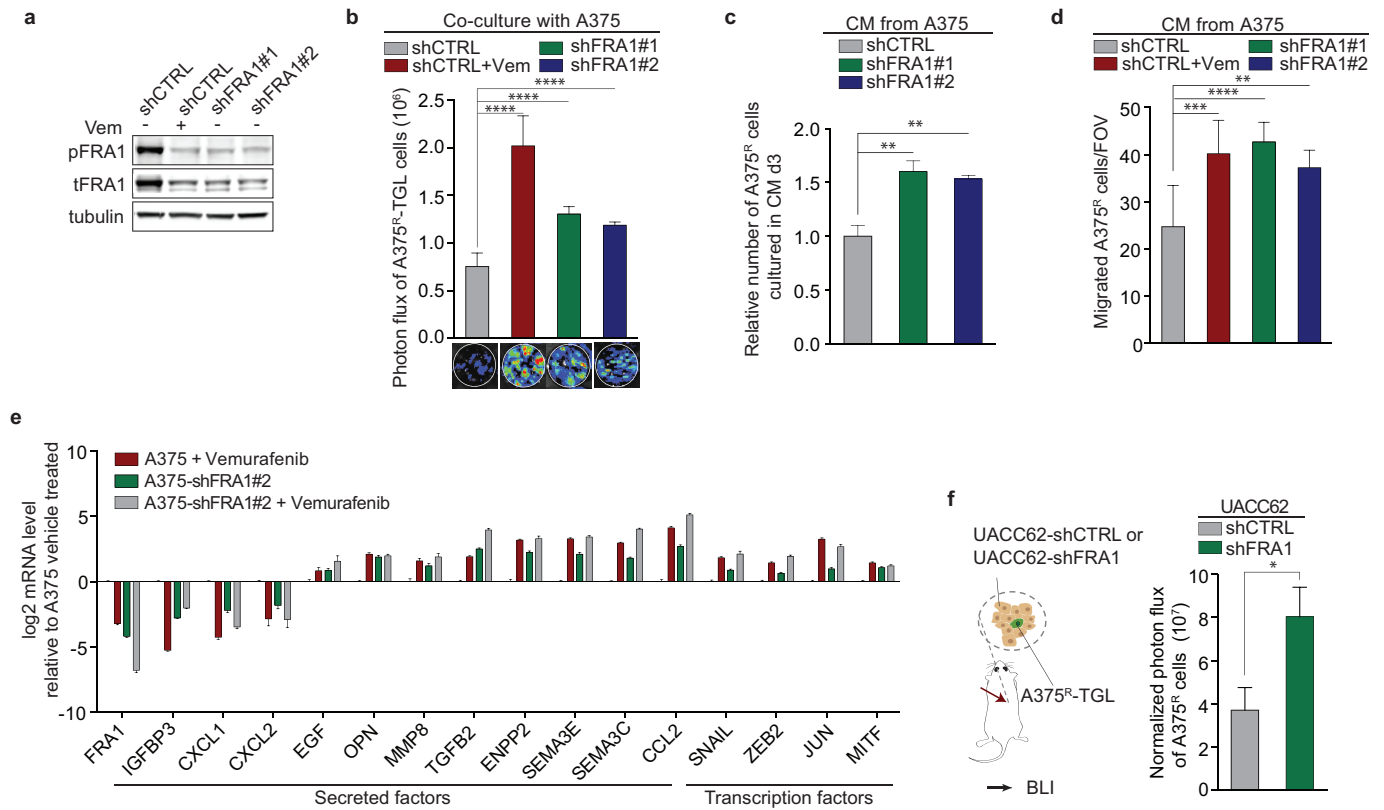
Extended Data Figure 4 | Vemurafenib treatment induces widespread changes in the intra-tumour immune cell composition and stromal cytokine composition in tumours regressing during targeted therapy. **a, b**, FACS analysis of murine immune cell populations in A375-derived xenograft tumours treated with vehicle or vemurafenib for 5 days. **a, b**, Representative image (**a**) and quantification (**b**) of intra-tumour composition of indicated

immune cell populations (vehicle, $n = 4$; vemurafenib, $n = 6$ tumours). **c, d**, Cytokine array of murine stroma-derived cytokines within A375-derived xenograft tumours treated with vehicle or vemurafenib for 5 days. Representative image (**c**) and quantification (**d**) of down- and upregulated cytokines ($n = 4$ tumours). P values calculated by a two-tailed Mann-Whitney U test. Data are mean and s.e.m.



Extended Data Figure 5 | Targeted therapy induces downregulation of FRA1 in drug-sensitive tumour cells. **a**, List of transcription factors predicted to regulate the vemurafenib-induced reactive secretome in A375 cells, and a heat map of the corresponding transcription factor gene expression levels in these cells. Red represents high, yellow medium and blue low relative expression on the colour scale. **b**, Immunoblotting of phosphorylated and total FRA1 protein levels in A375 and YUMM1.7 melanoma cell lines treated with vemurafenib for 24 h. **c**, Relative mRNA levels of *FRA1* in H3122 cells

treated with crizotinib (500 nM) and HCC827 treated with erlotinib (10 nM) at different time points ($n = 4$ technical replicates). **d**, Relative mRNA levels of *FRA1* in A375^R cells treated with vemurafenib at different time points ($n = 4$ technical replicates). **e**, Immunofluorescence staining of FRA1 (red) and DAPI (blue) in biopsies from melanoma patients before and after vemurafenib treatment (clinical information can be found in Extended Data Table 1). Original magnification, $\times 20$.



Extended Data Figure 6 | The secretome of melanoma cells with FRA1 knockdown stimulates proliferation and migration of A375^R cells in vitro and in vivo. **a**, Immunoblotting of phosphorylated and total FRA1 protein levels in A375 cells transduced with control shRNA, with or without additional vemurafenib treatment, or shRNAs targeting FRA1. **b**, Photon flux and representative BLI images of TGL-expressing A375^R cells co-cultured with A375 cells expressing control shRNA (with or without vemurafenib treatment) or FRA1-targeting shRNAs after 7 days ($n = 9$ biological replicates). **c**, Relative number of A375^R cells after 3 days in the presence of conditioned media derived from A375 cells transduced with control shRNA, with or without additional vemurafenib treatment, or FRA1 shRNAs ($n = 3$ biological replicates).

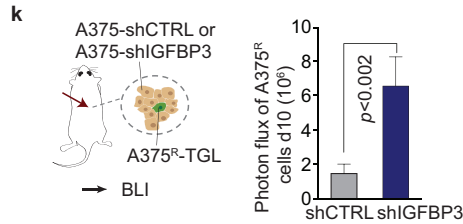
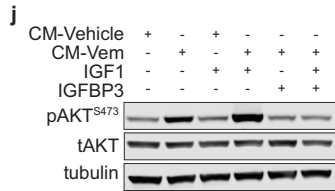
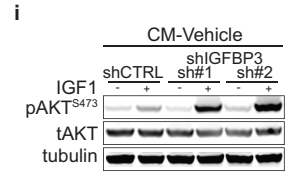
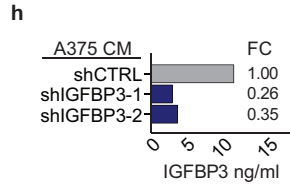
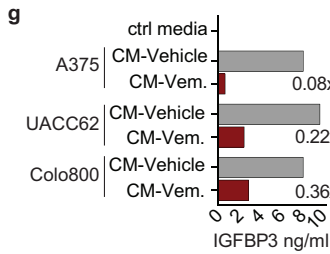
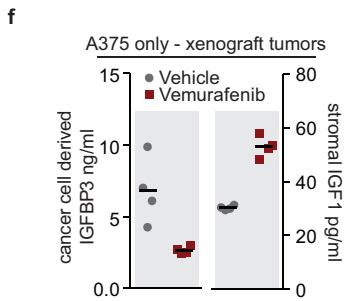
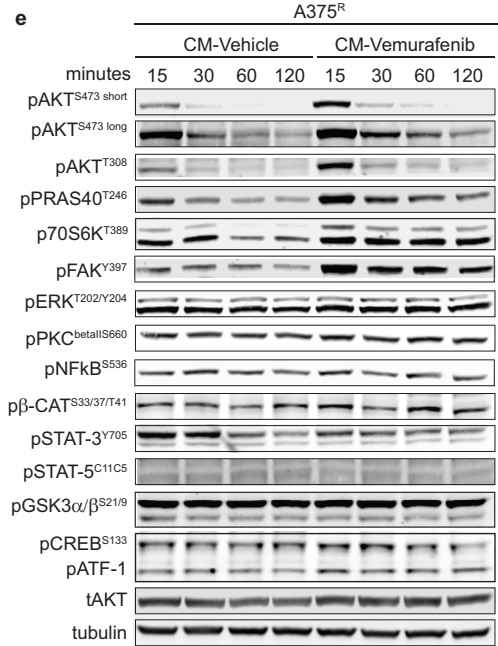
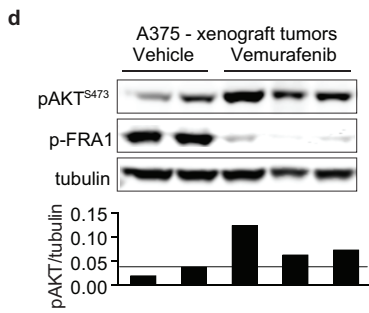
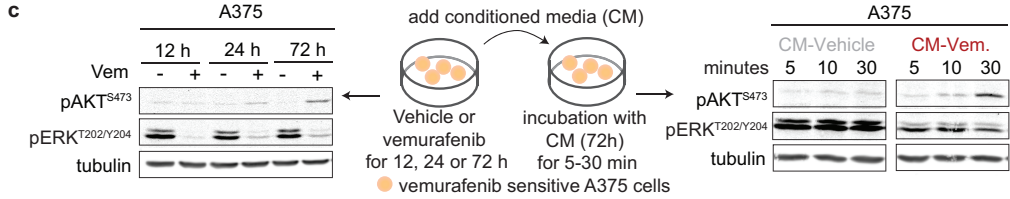
d, Migration of A375^R cells towards conditioned media derived from A375 cells transduced with control shRNA (with or without vemurafenib treatment) or FRA1 shRNAs using a Boyden chamber assay (shCtrl, $n = 15$; all other groups $n = 10$ FOV) **e**, Relative mRNA levels of selected secreted factors and transcription factors of A375 cells expressing control shRNA or an shRNA targeting FRA1 (shFRA1-1), treated with vehicle or vemurafenib (24 h). **f**, Bioluminescent signal of A375^R-TGL cells 8 days after subcutaneous co-implantation with UACC62 cells expressing a control or an shRNA for FRA1 (shCtrl, $n = 12$; shFRA1, $n = 20$ tumours). Data are mean and s.e.m. * $P < 0.05$, ** $P < 0.01$, *** $P < 0.001$, **** $P < 0.0001$, Student's t -test.

a

Functions Annotation	p-Value	z-score
cell movement	3.28E-07	2.158
quantity of cells	7.49E-05	2.029
proliferation/tumor cell lines	1.73E-04	2.328
leukocyte migration	2.69E-04	2.456
cell survival	5.31E-04	2.363
homing	5.52E-04	2.410
cell viability	8.55E-04	2.438
chemotaxis	9.62E-04	2.194
organismal death	3.99E-05	-3.589
apoptosis/cancer cell lines	4.72E-03	-2.078

b

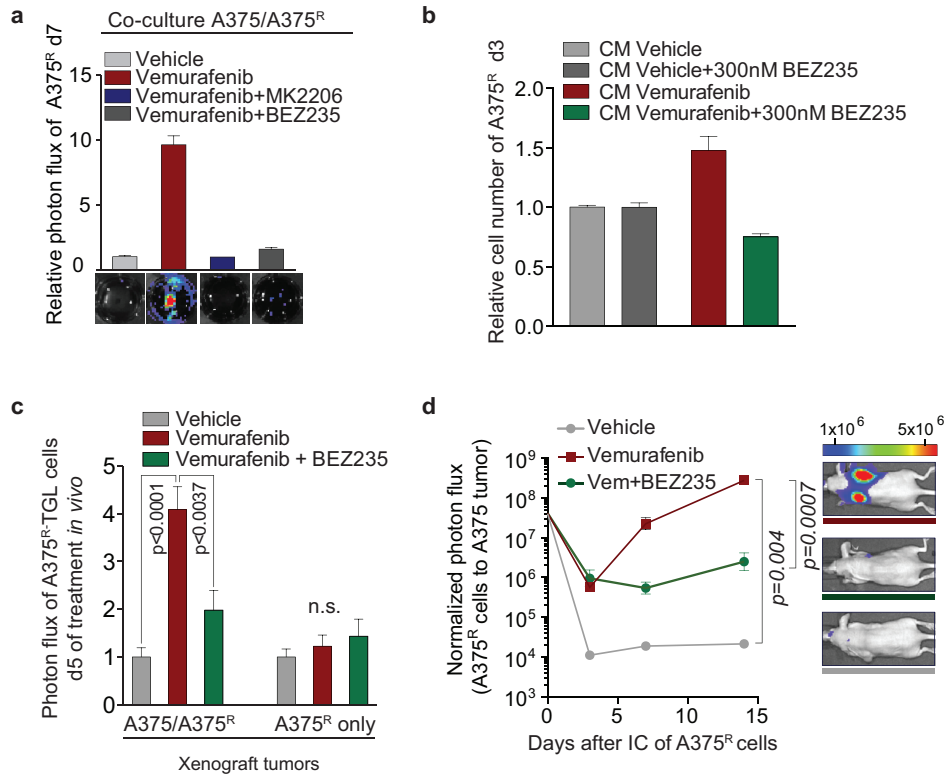
Target	Inhibitor	Z-Score	P-value
PI3K	LY294002	-2.287	2.87E-03
PKC	bisindolylmaleimide I	-2.200	1.26E-03
mTOR	sirolimus	-2.750	1.98E-02



Extended Data Figure 7 | The TIS includes upregulated positive regulators and a loss of negative regulators of the PI(3)K/AKT/mTOR pathway, which is activated in sensitive and resistant cells *in vitro* and *in vivo*.

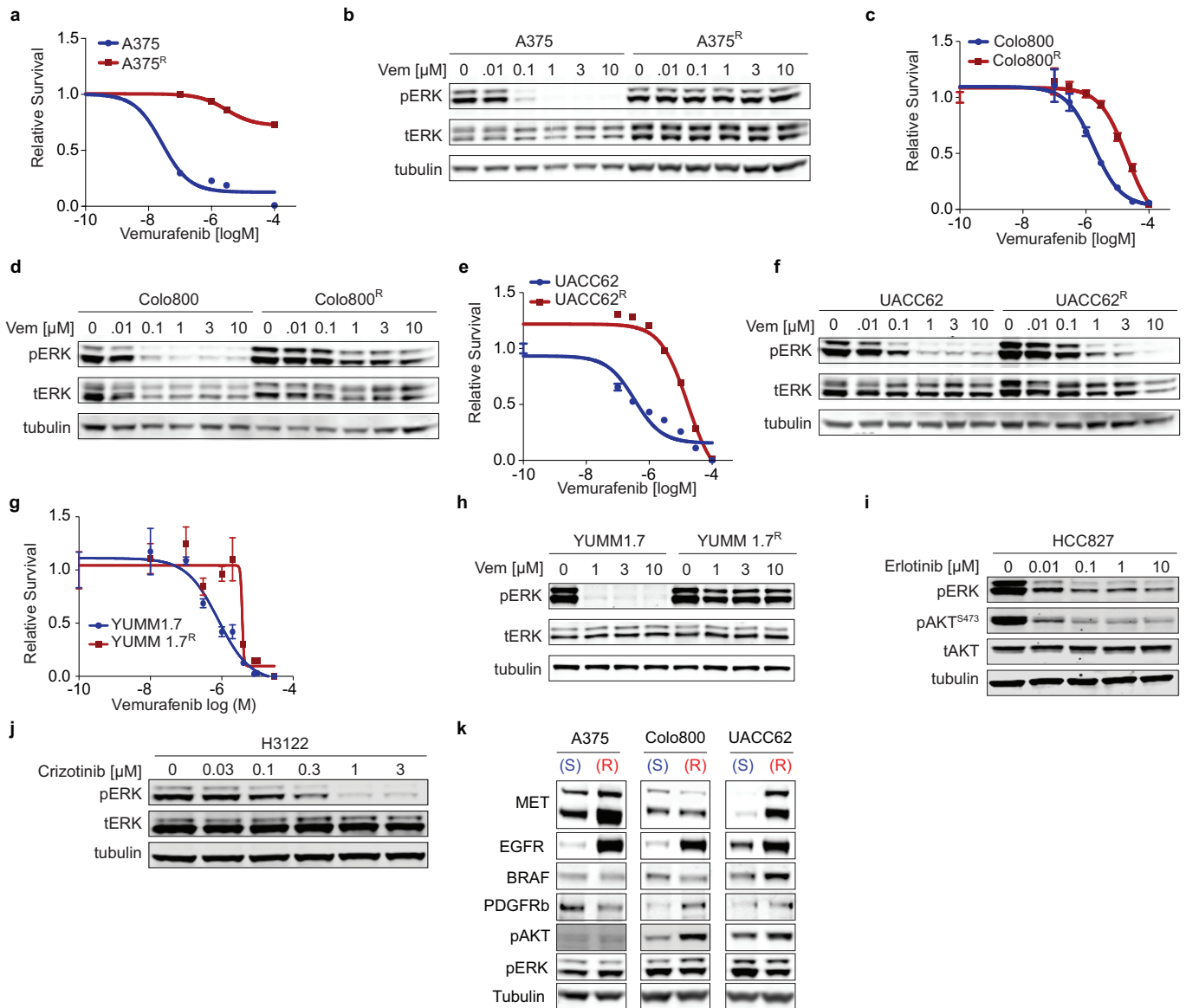
a, b, Enriched biological processes (**a**) and inferred drug vulnerabilities (**b**) as determined by Ingenuity pathway analysis of gene expression data from vemurafenib-resistant A375^R cells responding to signals from the reactive tumour microenvironment of a tumour regressing during targeted therapy *in vivo* (for experimental set-up see Fig. 1a and Methods). **c**, Left, immunoblotting of phosphorylated AKT^{S473} and phosphorylated ERK protein levels in A375 cells treated with vehicle or vemurafenib at different time points during the generation of conditioned media. Right, immunoblotting of phosphorylated AKT^{S473} and phosphorylated ERK protein levels in A375 cells after short-term exposure to conditioned media derived from A375 cells treated with vehicle or vemurafenib. **d**, Immunoblotting of phosphorylated AKT^{S473} and phosphorylated FRA1 protein levels in A375-derived xenograft tumours treated with vehicle or vemurafenib for 5 days. Normalized quantification of phospho-AKT^{S473}/tubulin in the bottom panel. **e**, Immunoblotting of a range of pathway nodes in A375^R cells treated with

CM-vehicle or CM-vemurafenib, derived from A375 cells, for 15, 30, 60 or 120 min. **f**, Cancer cell-derived IGFBP3 levels (left) and murine stromal IGF1 levels (right) in A375-derived xenograft tumours treated with vehicle or vemurafenib for 5 days as determined by ELISA ($n = 4$ tumours). **g**, Cancer-cell-derived IGFBP3 levels in conditioned media from indicated melanoma cell lines treated with vehicle or vemurafenib as determined by ELISA ($n = 3$ technical replicates of conditioned media derived from at least two biological replicates). **h**, IGFBP3 levels in conditioned media derived from A375 cells expressing control shRNA or shRNAs targeting *IGFBP3* (shIGFBP3-1 and -2) as determined by ELISA ($n = 3$ technical replicates). **i**, Immunoblotting of phosphorylated AKT^{S473} in A375^R cells after incubation with conditioned media of A375 cells expressing control shRNA or shRNAs targeting *IGFBP3*. **j**, Phosphorylation status of AKT^{S473} in A375^R cells after incubation for 15 min with conditioned media, IGF1 and IGFBP3 as indicated. **k**, Bioluminescent signal of A375^R-TGL cells 10 days after co-implantation with A375 cells expressing a control shRNA or an shRNA targeting *IGFBP3* (shIGFBP3-1) ($n = 10$ tumours). P values calculated by a two-tailed Mann–Whitney U test. Data are mean and s.e.m.



Extended Data Figure 8 | Dual inhibition of RAF and the AKT/mTOR pathway blunts the effects of the regressing tumour environment on the resistant cell population. **a**, Relative photon flux and representative BLI images of GFP/luciferase expressing A375^R cells co-cultured with A375 cells and treated with vehicle, vemurafenib or the combination of vemurafenib and either MK2206 (AKTi, 2 μ M) or BEZ235 (PI(3)K/mTORi, 300 nM) for 7 days ($n = 2-3$ biological replicates). **b**, Relative number of A375^R cells after 3 days in the presence of CM-vehicle or CM-vemurafenib with additional BEZ235 (300 nM) ($n = 3$ biological replicates). **c**, Mice bearing tumours consisting of A375/A375^R cells or A375^R cells alone were treated with drugs as indicated.

Bioluminescent signal of TGL-expressing A375^R cells was determined on day 5 of treatment ($n = 16, 16, 12, 12, 12$ and 16 tumours, respectively). **d**, Mice bearing tumours consisting of unlabelled A375 cells were pre-treated for 3 days with drugs as indicated and 1×10^5 TGL-expressing A375^R cells were inoculated in the arterial circulation. Drug treatment was continued and seeding of resistant cells to the primary tumour was quantified by BLI. Representative BLI images on the right (vehicle, $n = 4$; vemurafenib $n = 10$, vemurafenib plus BEZ235, $n = 10$ tumours). P values calculated by a two-tailed Mann-Whitney test. Data are mean and s.e.m.



Extended Data Figure 9 | Characterization of cell lines in response to targeted therapy. **a–h**, Relative survival of human melanoma cell lines (A375, Colo800 and UACC62) (**a**, **c**, **e**), and the murine melanoma cell line YUMM1.7 (**g**) and corresponding vemurafenib-resistant derivatives (A375^R, Colo800^R, UACC62^R and YUMM1.7^R) under increasing concentrations of vemurafenib. Immunoblotting of phosphorylated ERK protein levels in indicated melanoma cell lines in the presence of increasing concentrations of vemurafenib (**b**, **d**, **f**, **h**). **i**, Immunoblotting of phosphorylated ERK and

phosphorylated AKT^{S473} protein levels in HCC827 lung adenocarcinoma cells in the presence of increasing concentrations of erlotinib. **j**, Immunoblotting of phosphorylated ERK protein levels in H3122 lung adenocarcinoma cells in the presence of increasing concentrations of crizotinib. **k**, Immunoblotting of protein levels of MET, EGFR, BRAF, PDGFR β , phosphorylated AKT and phosphorylated ERK in vemurafenib-sensitive and -resistant pairs of human melanoma cell lines (A375, Colo800 and UACC62).

Extended Data Table 1 | Clinical data for tissue donor subjects

Study site	Pt #	Bx samples	Age & Sex	Stage	Dose (mg)	BOR	PFS (days)	Bx site
UCLA	1 TG	Baseline Day 7	51M	M1c	960 bid vemurafenib	-21%	108	SC, scalp SC, scalp
	2 JCC	Baseline Day 15	44M	M1c	960 bid vemurafenib +60 qd cobimetinib	-63%	Current response	SC, abdomen SC, abdomen
	3 YAU	Baseline Day 22	26F	M1c	960 bid vemurafenib +60 qd cobimetinib	-46%	145	Dermal/SC, abdomen Dermal/SC, clavicle

bid, twice daily; BOR, best overall response; Bx, biopsy; F, female; M, male; PFS, progression-free survival; Pt, patient; qd, daily; SC, subcutaneous; UCLA, University of California, Los Angeles.